Title

Autocrine VEGF maintains endothelial survival through regulation of metabolism and autophagy

Journal

Journal of Cell Science, 128(12)

ISSN

0021-9533

Authors

Domigan, Courtney K
Warren, Carmen M
Antanesian, Vaspour
et al.

Publication Date

2015-06-15

DOI

10.1242/jcs.163774

Peer reviewed

© 2015. Published by The Company of Biologists Ltd | Journal of Cell Science (2015) 128, 2236-2248 doi:10.1242/jcs.163774

RESEARCH ARTICLE

Autocrine VEGF maintains endothelial survival through regulation of metabolism and autophagy

Courtney K. Domigan[1], Carmen M. Warren[1], Vaspour Antanesian[1], Katharina Happel[2], Safiyyah Ziyad[1], Sunyoung Lee[1], Abigail Krall[4], Lewei Duan[5], Antoni X. Torres-Collado[1], Lawrence W. Castellani[6], David Elashoff[5], Heather R. Christofk[4], Alexander M. van der Bliek[7,8], Michael Potente[2] and M. Luisa Iruela-Arispe[1,3,7,*]

ABSTRACT

Autocrine VEGF is necessary for endothelial survival, although the cellular mechanisms supporting this function are unknown. Here, we show that – even after full differentiation and maturation – continuous expression of VEGF by endothelial cells is needed to sustain vascular integrity and cellular viability. Depletion of VEGF from the endothelium results in mitochondria fragmentation and suppression of glucose metabolism, leading to increased autophagy that contributes to cell death. Gene-expression profiling showed that endothelial VEGF contributes to the regulation of cell cycle and mitochondrial gene clusters, as well as several – but not all – targets of the transcription factor FOXO1. Indeed, VEGF-deficient endothelium *in vitro* and *in vivo* showed increased levels of FOXO1 protein in the nucleus and cytoplasm. Silencing of FOXO1 in VEGF-depleted cells reversed expression profiles of several of the gene clusters that were de-regulated in VEGF knockdown, and rescued both cell death and autophagy phenotypes. Our data suggest that endothelial VEGF maintains vascular homeostasis through regulation of FOXO1 levels, thereby ensuring physiological metabolism and endothelial cell survival.

KEY WORDS: Vascular biology, FOXO1, Signal transduction

INTRODUCTION

Development of vascular networks requires paracrine stimulation of the endothelium through VEGF to induce growth and branching, which cannot be accomplished when even a single VEGF allele is ablated (Ferrara et al., 1996; Carmeliet et al., 1996). However, autocrine VEGF expressed by the endothelium itself is optional for this particular process. Mice with deletion of VEGF in the endothelial compartment, i.e. VEGF endothelial cell knock out (VEGF-ECKO) animals, are largely viable and develop vasculature of normal appearance and density (Lee et al., 2007). What is apparent in the VEGF-ECKO, however, is that over time they suffer from vascular degeneration resulting in premature death from strokes and hemorrhage (Lee et al., 2007). These results imply a unique role for autocrine VEGF signaling: although autocrine VEGF is dispensable for the development of vessels, it is required for maintenance of endothelial viability.

Further straying from the actions of paracrine VEGF, which interacts with receptors at the cell surface, autocrine VEGF signaling occurs, at least in part, within the cell. Cell death in VEGF-deficient endothelium cannot be rescued by addition of exogenous VEGF, or even by co-culture with WT endothelium – that could presumably supply endothelial-derived VEGF to neighboring cells (Lee et al., 2007). These experiments suggest that VEGF, in a cell-autonomous manner, contributes to cell survival in a way that is independent of surface ligand/receptor interactions. These cell-autonomous responses are not exclusive to the endothelium, and have been also shown in hematopoietic cells (Gerber et al., 2002) and in some tumor cells (Lichtenberger et al., 2010; Samuel et al., 2010).

Whereas endothelial responses to paracrine VEGF is well characterized, the signaling effects of autocrine VEGF are not well understood. For example, it has been observed that the endothelium upregulates VEGF in response to hypoxia *in vitro* (Namiki et al., 1995) and in several vascular beds *in vivo* (Maharaj et al., 2006; Lee et al., 2007; dela Paz et al., 2012); but to what purpose? In situations of tumor or organ growth, hypoxia-induced VEGF in tumor cells or other vascular-adjacent cells acts primarily as the chief paracrine source that elicits recruitment of blood vessels (Matsumoto and Claesson-Welsh, 2001), but the needs of the endothelium itself are quite different. Stable vessels experiencing hypoxia are not thought to undergo proliferation or remodeling and, instead, they must adjust their metabolic state to survive the cellular stress.

Paracrine VEGF promotes migration and proliferative responses. This is in contrast to autocrine VEGF signaling, which is poorly understood although endothelial VEGF is associated with upregulation of survival genes (Franco et al., 2011; Fan et al., 2014). Because autocrine VEGF appears to be required for cell survival in situations of stress, we sought to investigate the specific cellular processes regulated by autocrine VEGF in endothelial cells.

RESULTS

Endothelial VEGF prevents vascular injury under hypoxic conditions

The need for cell-autonomous VEGF signaling in endothelial homeostasis has been demonstrated previously by using a constitutive deletion model that results in sudden death of a large proportion of adult animals (Lee et al., 2007). Because the sudden-death phenotype was not completely penetrant, we postulated that VEGF is required for protection from certain types of stress that may incidentally occur in the adult. As endothelial VEGF expression is

[1]Department of Molecular, Cell and Developmental Biology, University of California, Los Angeles, CA 90024, USA. [2]Angiogenesis and Metabolism Laboratory, Max Planck Institute for Heart and Lung Research, 61231 Bad Nauheim, Germany. [3]Molecular Biology Institute, University of California, Los Angeles, CA 90024, USA. [4]Molecular and Medical Pharmacology, University of California, Los Angeles, Los Angeles, CA 90024, USA. [5]Department of Medicine Statistics Core, University of California, Los Angeles, Los Angeles, CA 90024, USA. [6]Department of Medicine, University of California, Los Angeles, CA 90024, USA. [7]Jonsson Comprehensive Cancer Center, University of California, Los Angeles, CA 90024, USA. [8]Biological Chemistry, University of California, Los Angeles, Los Angeles, CA 90024, USA.

*Author for correspondence (arispe@mcdb.ucla.edu)

Received 23 September 2014; Accepted 30 April 2015

Journal of Cell Science

Journal of Cell Science (2015) 128, 2236-2248 doi:10.1242/jcs.163774

increased under hypoxic conditions (Namiki et al., 1995), we tested the effects of low oxygen levels on Cre recombinase (Cre)-negative (controls) and VEGF-ECKO animals.

A cohort of VEGF-ECKO (n=24) and control (n=19) mice aged 8–12 weeks was exposed to intermittent hypoxia over a 5-week period. During this treatment period, three VEGF-ECKO deaths were recorded whereas the control group remained 100% viable. Directly after completion of the final treatment, all animals were harvested and assessed histologically for vascular-related lesions of the most affected organs (as described in Lee et al., 2007). At baseline, histological analysis of VEGF-ECKOs revealed intestinal perforations, brain hemorrhage and heart fibrosis indicative of loss of vascular integrity (Fig. 1A), similar to results reported previously (Lee et al., 2007). However, the severity and penetrance of the injuries was highly increased once these animals were placed under hypoxic conditions. Evaluation of control and VEGF-ECKO mice under both conditions showed that, whereas incidence of at least one of those pathologies was noticed in 64.3% of VEGF-ECKO mice under normoxia, 91% of this group were affected under hypoxic conditions. Control animals were entirely protected from injury in the presence of endogenous VEGF during either normoxia or hypoxia (Fig. 1A). Interestingly, we found that, although all lesion types were increased upon exposure of VEGF ECKO mice to hypoxia, the cardiac vascular beds were particularly susceptible to removal of VEGF (Fig. 1B). These results suggest that, rather than recruit the growth of new vessels, the upregulation of endothelial VEGF prevents the onset of vascular lesions.

Autocrine VEGF is required continuously to maintain vascular integrity

A caveat of the VEGF-ECKO model of constitutive deletion was the intrinsic difficulty to discern whether VEGF excision from the onset of endothelial specification carried developmental rather than homeostatic consequences to adult mice. Hypothetically, VEGF may be required in a small developmental time window for endothelial differentiation, after which it is no longer necessary. To discern between the need of VEGF in vascular homeostasis from its 'developmental' role, we generated an inducible model of deletion of VEGF in the endothelium. Tamoxifen-inducible deletion of VEGF in endothelial cells was accomplished by generating a new mouse line (referred to as VEGF-iECKO) that carries an inducible VE-CAD Cre transgene in the background of VEGF lox/lox. VEGF deletion in response to tamoxifen treatment in young adult mice resulted in sudden death of 33% of these animals by 50 weeks, indicating that autocrine VEGF is, indeed, required for homeostatic function of the adult endothelium (Fig. 1C).

To define the requirement for continuous endothelial VEGF at the cellular level, we isolated endothelium from floxed-VEGF adults,

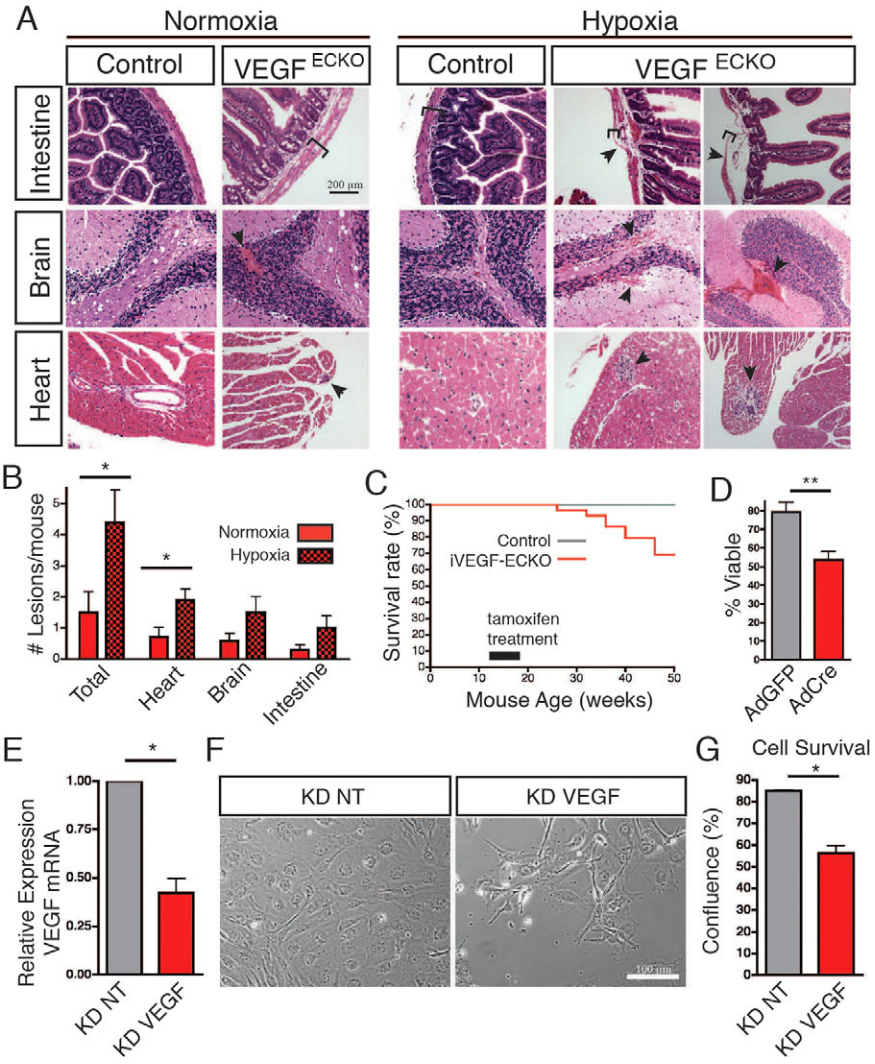

Fig. 1. Continuous presence of autocrine VEGF is required for endothelial cell survival. (A) H&E-stained histological sections of VEGF-ECKO mice after hypoxia treatment. Arrowheads indicate areas of hemorrhage. Brackets indicate thickness of outer intestinal wall. (B) Quantification of A showing average number of lesions per VEGF-ECKO mouse under conditions of normoxia or hypoxia. No lesions were observed in control mice (VEGF-ECKO: n=14 normoxia, n=10 hypoxia; Control: n=9 normoxia, n=10 hypoxia). (C) Survival analysis of iVEGF-ECKO mice after tamoxifen injection at 10 weeks. Sudden death starting 15 weeks post-injection (Control n=25, iVEGF-ECKO n=30). (D) Viability of endothelium isolated from the liver of adult floxed-VEGF mice treated in culture with adenoviral GFP (Ad-GFP) or Cre (Ad-Cre) (n=6). (E) siRNA targeting VEGF results in a more than 50% decrease of VEGF transcript (n=3). (F) KD-VEGF reduces cell viability. Images were collected from the cell layer 5 days after the first transfection. Scale bar, 100 μm. (G) Quantification of cell confluence from F (n=4). For all graphs, error bars indicate the mean±s.d.; *P<0.05, **P<0.005.

Journal of Cell Science

Journal of Cell Science (2015) 128, 2236-2248 doi:10.1242/jcs.163774

and then ablated VEGF in culture by adeno-Cre exposure (Fig. 1D). We found that, even after normal differentiation in a phenotypically WT environment (VEGF lox/lox Cre-negative), ablation of VEGF *in vitro* resulted in decreased cellular viability (Fig. 1D). We further assessed the role of autocrine VEGF in a human endothelial cell model by depletion of VEGF from a confluent HUVEC monolayer. We subjected HUVECs to small interfering RNA (siRNA)-meditated knockdown of VEGF (KD-VEGF) and found that a reduction in VEGF transcripts (~50%; Fig. 1E) resulted in a striking loss of cells compared to controls after 3 days (Fig. 1F,G), indicating high levels of cell death. Together, these results suggest that endothelial VEGF is required continuously for cell survival at the organismal level *in vivo* and at the cellular level *in vitro*.

Endogenous VEGF sustains endothelial cell viability and survival through signaling initiated in an intracellular compartment

Although endogenous VEGF is clearly required for survival, we sought to determine whether the signaling responsible for maintenance of viability is analogous to the well-studied cell surface pathway or, whether signaling occurs through a different intracellular pathway. To answer this question, we first evaluated secreted and intracellular levels of VEGF in endothelial cells. Using a sensitive ELISA assay, we compared the levels of VEGF secreted from a confluent layer to those retained within the cells themselves (Fig. 2A). An endothelial cell panel consisting of HUVECs, human dermal micro-endothelial Cells (HDMECs) and hemangioma endothelial cells (HemEC) were compared to a panel of tumor cells (T47D, MCF7, MDAMB and SW480). In contrast to non-transformed cells, we looked at a panel of cell lines from normal primary tissues including endometrial epithelial cells (Endo. Epithel), human umbilical mesenchymal stem cells (HUMSC) and myofibroblasts. We found that, although the levels of VEGF produced by endothelial cells were very low, a relatively large proportion of the protein (on average 60% retention) was retained within the endothelial cells. This was in stark contrast to non-transformed primary cells and tumor lines that retain only 1–8% of the VEGF made (Fig. 2A).

To test whether the endogenous internal VEGF is biologically relevant for cell survival, we exposed WT HUVECs to internal and external blockade of VEGF under serum-starved conditions. Anti-VEGF antibody was used to block extracellular VEGF, whereas internal and external signaling of VEGF receptor 2 (VEGFR2) was blocked by using the small-molecule inhibitor SU4312. HUVECs treated with a high dose of anti-VEGF antibody remained similarly viable compared with non-treated cells, whereas SU4312-treated cell cultures showed a drastic reduction in cell confluence (Fig. 2B), similar to KD-VEGF cells (Fig. 1G).

Cells were treated with saturating doses of inhibitors sufficient to block the signaling effects of even large amounts of exogenous recombinant VEGF (rVEGF), far in excess of endogenous VEGF

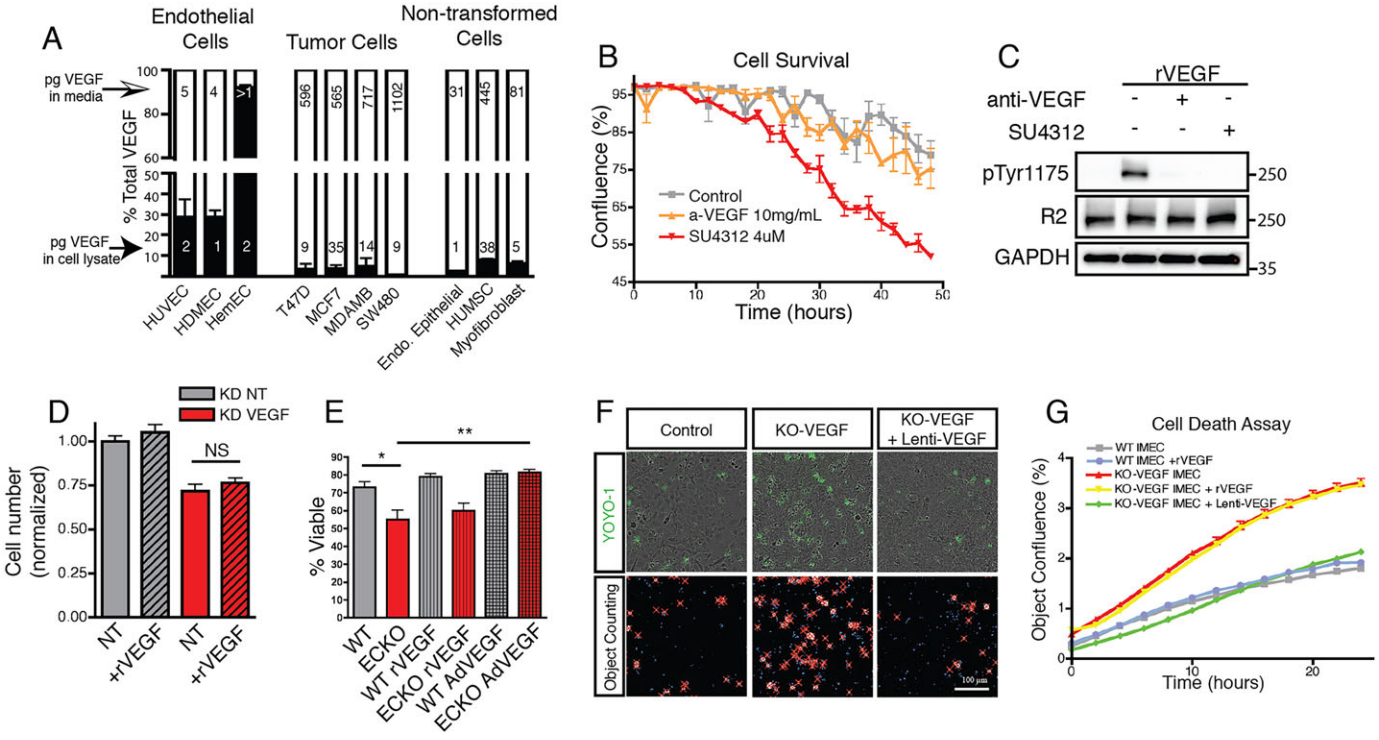

Fig. 2. Reduction or inactivation of endothelial VEGF results in cell demise. (A) Secreted and intracellular VEGF levels after 24 h were measured by ELISA. Numbers at top and bottom of graph indicate the total levels of VEGF (as average VEGF in pg per well) from a confluent 6-well plate in medium or cell lysate (n=3–6). (B) Quantification of HUVEC survival over time during serum starvation ('C', control, gray), extracellular blockade of endogenous VEGF (B20 at 10 µg/ml, orange) or inhibition of intra- and extracellular activation of VEGFR2 (SU4312 at 4 µM, red). (C) Western blot analysis. Phosphorylation of VEGFR2 at Tyr1175 is efficiently blocked in rVEGF-treated (10 mg/ml) WT HUVECs when incubated with either anti-VEGF antibody (B20, 10 µg/ml) or the cell-permeant VEGFR2 (R2) inhibitor (SU4312, 4 µM). Numbers on the right indicate molecular mass in kDa. (D) Cellular viability of HUVECs after knockdown of VEGF by using siRNA is not rescued by addition of exogenous rVEGF throughout the experiment (n=3). NT, non-target control; NS, not significant. (E) Viability of endothelial cells isolated from adult WT or VEGF-ECKO mice treated with exogenous rVEGF (100 ng/ml) or infection with adenoviral VEGF (n=10), *P<0.05, **P<0.0005. (F) Top row: representative images of cell death in HUVECs cell death is indicated by fluorescent signals of YOYO-1. Bottom row: examples of object counting used for quantification (red crosses). Scale bar: 100 µm. (G) Cell death assessed over 24 h by using YOYO-1 in WT or KO-VEGF mouse endothelium, either untreated or treated with rVEGF (100 ng/ml), or infected with lentiviral-VEGF, n=9.

Journal of Cell Science

Journal of Cell Science (2015) 128, 2236-2248 doi:10.1242/jcs.163774

levels. To demonstrate the robustness of the inhibition, we treated WT HUVECs with a high concentration of rVEGF (100 ng/ml) and either with or without VEGF2 inhibitor (SU4312) or antibody against VEGF (B20), and probed for phosphorylation of VEGFR2 at Tyr1175, a main VEGF-dependent auto-phosphorylation site (Fig. 2C). Both treatments completely prevented phosphorylation of Tyr1175 due to this high dosage of exogenous VEGF, and readily overcame signaling resulting from the low levels of endogenous endothelial VEGF. Together, these results suggest that endothelial cells are dependent on an endogenous intracellular source of VEGF for their survival.

Throughout these experiments, a relatively trivial explanation to the findings is that loss of VEGF from the endothelial compartment decreases the local supply of VEGF available to the cell, thus restricting signaling of surface receptors. To explore whether loss of autocrine VEGF can be rescued by simple supplementation of exogenous VEGF, rVEGF was added to confluent cultures that had been previously exposed to siRNA KD-VEGF to remove endogenous stores (Fig. 2D). Addition of daily exogenous VEGF throughout the 5-day knockdown procedure did not alleviate the cell death phenotype. It should be noted that, whereas VEGF is a potent mitogen, addition of rVEGF to non-targeting siRNA (KD-NT) did not result in an increase in cell numbers because the experiment was performed in a confluent monolayer of cells. We also assessed cell viability *in vitro* with endothelium isolated from VEGF-ECKO adult mice in the presence and absence of exogenous VEGF. Again, the cell viability defect of VEGF-ECKO could not be rescued by addition of exogenous rVEGF (Fig. 2E). In contrast, infection of VEGF-ECKO cells with adeno-VEGF increased viability to WT levels (Fig. 2E). This result suggests that rescue can only occur if VEGF is delivered intracellularly and that an endothelial source of VEGF, rather than just the total amount, is essential.

The determination of cell viability in murine ECKO cells could not perfectly distinguish between decrease in proliferation or promotion of cell death, thus we sought to directly investigate the rate of cell death in a confluent monolayer of cells that had lost VEGF expression. Increased cell death was confirmed using endothelial cells derived from VEGF lox/lox mice exposed to adeno-Cre *in vitro* to generate VEGF-knockout (KO-VEGF IMEC) and relative control (WT IMEC) endothelium. Cell death was assessed in real time by using a cell-impermeant DNA dye in 2-hour increments over 24 h and we observed that KO-VEGF mouse endothelial cultures had a high incidence of cell death during serum starvation when compared to cultures with wild-type levels of VEGF (Fig. 2F,G). To test whether extracellular VEGF can rescue this phenotype, KO-VEGF murine endothelial cells were further treated with exogenous rVEGF, which did not significantly alter viability (Fig. 2G). However, infection of KO IMECs with lentiviral VEGF resulted in a clear rescue of phenotype and decrease in cell death with numbers that approached WT levels (Fig. 2F,G), suggesting that VEGF is directly expressed by the endothelium itself and it has cell-autonomous effects.

Lack of VEGF results in mitochondrial fragmentation and metabolic collapse

To further clarify the specific mechanism of cell demise, we first evaluated apoptosis. Interestingly, in cell culture, classic indicators of apoptosis, such as cleaved caspase 3 and cleaved PARP, were not easily detected in KD-VEGF cells, although they could be induced by treatment with staurosporine (positive control; see supplementary material Fig. S1A,B). We additionally performed TUNEL assays on KD-VEGF and control cells and, although we saw a few TUNEL-positive cells, we found that the number of TUNEL-positive nuclei was equivalent to the number of cells lost in the absence of VEGF (supplementary material Fig. S1C).

To help assess the possible mode of cellular death, we performed microarrays on KD-NT and KD-VEGF cells to assess global changes in transcriptional. A database for annotation, visualization and integrated discovery (DAVID) analysis revealed downregulation of Golgi- and blood-vessel gene clusters (supplementary material Fig. S2A,B), and significant upregulation of a strongly represented mitochondrial gene cluster that shows a predominance in structural and housekeeping genes (Fig. 3A). This finding prompted us to examine mitochondrium structure and function in KD-NT and KD-VEGF cells. Staining with HDP60 in KD-NT cells, revealed the characteristic tree-like morphology of mitochondria that is typical for endothelial cells; in contrast, KD-VEGF cells showed drastic mitochondrial fragmentation (Fig. 3B). However, total levels of mitochondria were unchanged when VEGF was deleted, as shown by western blot analysis of HSP60 (Fig. 3C). The strong representation of mitochondrial structural and housekeeping genes (such as MRPL42, MRPL52, HIBCH, VPS25) suggests a possible compensatory mechanism where the cell may be attempting to counteract mitochondrial fragmentation.

One pathway of particular interest is that of cardiolipin synthesis and transport, which is represented by two of the top ten mitochondrial genes with the greatest fold-change in expression. Cardiolipin is a mitochondrium-specific glycerophospholipid that prevents apoptosis in several ways, including sequestration of cytochrome *c* in the mitochondrial inner membrane (Potting et al., 2013). HCLS1 is a synthase involved in the final step of cardiolipin synthesis (Chen et al., 2006) and TRIAP1 is a p53-regulated factor that is involved in the transfer of cardiolipin into the inner mitochondrial membrane (Potting et al., 2013). Interestingly, levels of MTX2, a protein that may act to sequester Bak from inducing apoptosis, are also increased (Cartron et al., 2014). The strong upregulation of these factors suggests an attempt to strengthen the mitochondrial membrane.

Based on the evident alteration in mitochondrial homeostasis, we evaluated the metabolic status of WT and KO-VEGF endothelial cells. Absence of VEGF resulted in a reduction of metabolic activity, in that glucose uptake, lactate production and triglyceride synthesis were all decreased (Fig. 3D,E,H). Suspecting additional metabolic effects, we investigated cellular oxygen consumption and mitochondrial respiratory capacity. Our findings indicate an overall depression of mitochondrial function (Fig. 3F,G). Furthermore, except for the case of triglyceride synthesis, all of these phenotypes manifested during both serum starvation and in the presence of serum, which frequently – but not in this case – compensate for small metabolic defects with an abundance of nutrients (Fig. 3D–H). Together, these results suggest that autocrine VEGF maintains normal metabolism in endothelial cells, without which the endothelium is challenged to survive.

Endogenous VEGF suppresses autophagic cell death

A common compensatory mechanism in dying cells attempting to mitigate life-threatening metabolic needs is to obtain nutrients through increased autophagy. We observed a marked increase in autophagic vacuoles in KD-VEGF HUVECs suggesting over-activation of autophagy (Fig. 4A,B). Although autophagic vacuoles were observed in a subset of KD-NT cells (Fig. 4Aa,Ac), the total number of cells with autophagic vacuoles was greater in the KD-VEGF population (Fig. 4Ad–Af). Biochemically, we saw an increase in total LC3A, which indicates an overall increase in autophagic

Journal of Cell Science (2015) 128, 2236-2248 doi:10.1242/jcs.163774

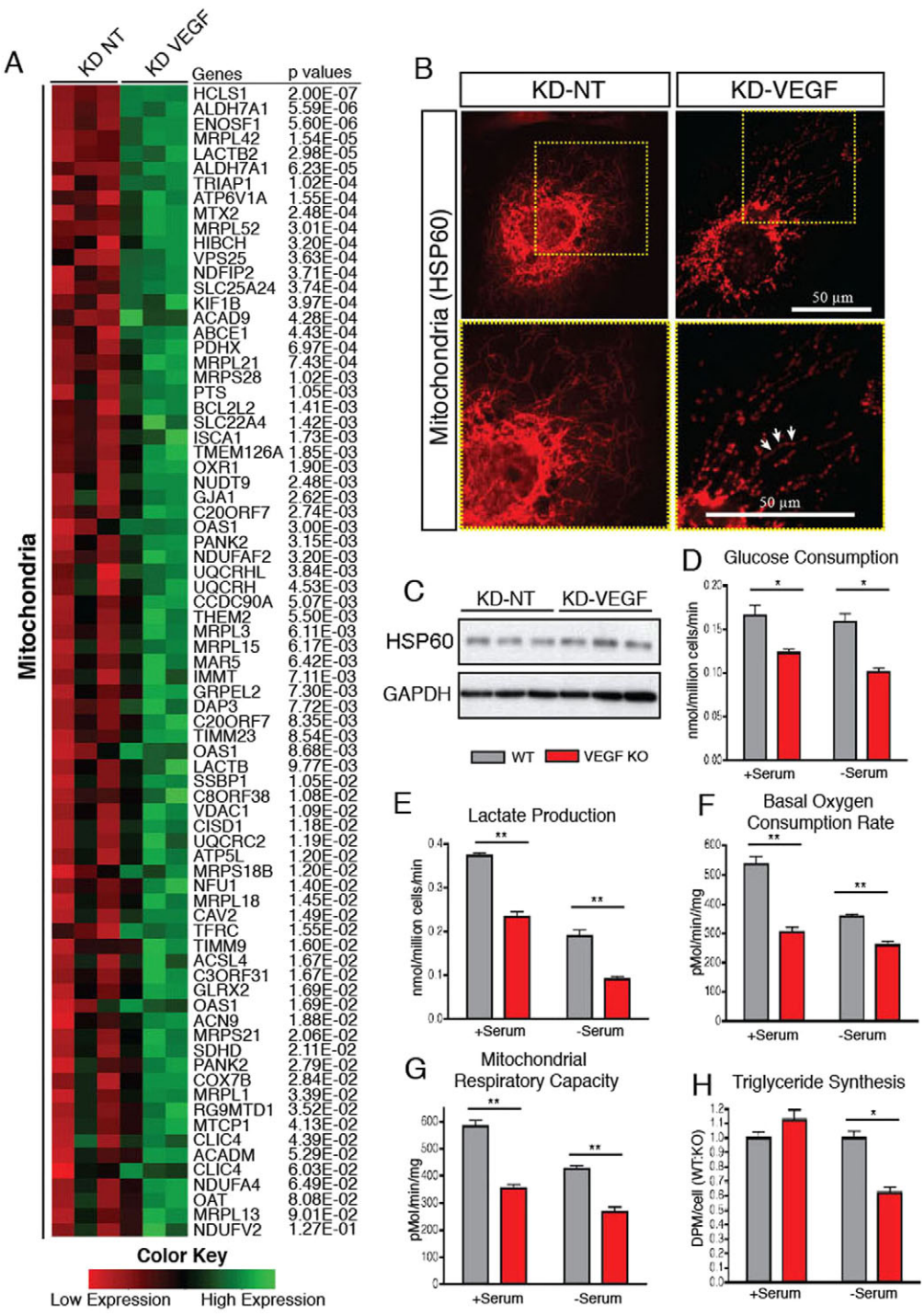

Fig. 3. Inactivation of endothelial VEGF results in metabolic deficiencies and mitochondrial fragmentation. (A) Microarray analysis showing expression patterns of KD-VEGF and control HUVECs reveal changes in the expression of mitochondrial GO clusters by DAVID analysis. (B) Hsp60 immunocytochemistry reveals mitochondria in KD-Scr and KD-VEGF HUVECs. Arrows indicate mitochondrial fragmentation. (C) The total volume of mitochondria is unchanged upon deletion of VEGF, as per levels of Hsp60 shown in western blots. (D–H) KO-VEGF mouse endothelial cells display decreased glucose uptake (D), lactate production (E), basal oxygen consumption (F) and mitochondrial respiratory capacity (G) measured in the presence or absence of serum (n=6). Triglyceride synthesis is decreased in KO-VEGF cells only under conditions of serum starvation (H) (n=4). For all graphs, error bars indicate the mean±s.d., *P<0.05; **P<0.005.

activity in KD-VEGF cells (Fig. 4C,D). We did not, however, observe increased turnover of LC3AI into LC3AII, suggesting that, although the number of autophagic vacuoles is increased, the rate of autophagic flux is unchanged on a per-vacuole basis (Fig. 4E).

To determine whether increase in autophagy occurred *in vivo*, we examined the ultrastructure of WT and VEGF-ECKO littermate control endothelium and compared the prevalence of autophagic vacuoles. EM images of *in vivo* micro-vasculature were examined for double-membrane structures characteristic of autophagosomes, or multi-membrane structures characteristic of later-stage autolysosomes (Mizushima et al., 2010). VEGF-ECKO endothelium had a higher incidence of autophagic vesicles that were not readily observed in WT endothelium (Fig. 4F). It is also interesting to notice the ultrastructure of VEGF-ECKO endothelium, which shows abundant cellular blebbing in contrast to its WT counterpart endothelium (Fig. 4F).

Because increased autophagy contributes to cell death in some contexts (Zhao et al., 2010), we inhibited the autophagic pathway and checked for rescue of cell death in KD-VEGF cells. We found that both silencing of the *Atg7* gene as well as pharmacologically blocking it with chloroquine (which inhibits lysosome acidification and fusion with autophagosomes) resulted in significant rescue of KD-VEGF cell death (Fig. 4G,H). Thus, disabling autophagy significantly increases cell survival in mutant cells, suggesting that autophagic cell death directly contributes to the KD-VEGF phenotype.

Journal of Cell Science (2015) 128, 2236-2248 doi:10.1242/jcs.163774

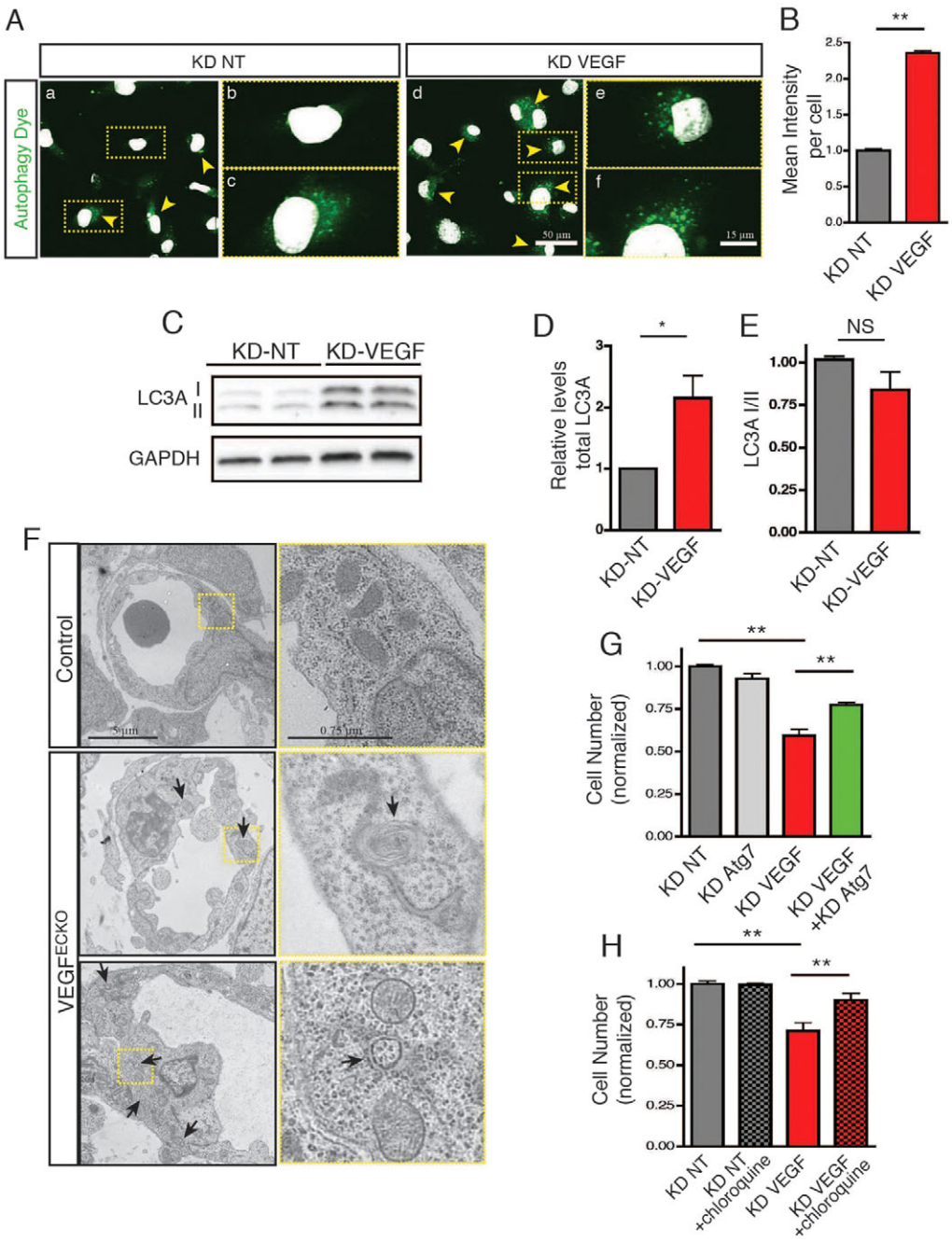

Fig. 4. Increased autophagy in VEGF-depleted endothelium contributes to cell death phenotype. (A) Autophagic vacuoles (arrowheads) visualized by using the Cyto-ID autophagy detection kit and analyzed by using a confocal microscope. (B) Quantification of fluorescence from cultures analogous to the ones shown in A (*n*=3). (C) Western blot of autophagic marker LC3A. (D) Quantification of total LC3A (LC3AI and LC3AII) levels normalized to GAPDH (*n*=8). (E) Autophagic flux measured by quantification of the LC3AI:LC3II ratio in western blots, (*n*=8). (F) Electron microscopy images. VEGF-ECKO adult animals display an abundance of double-membrane autophagic vacuoles (arrows). (G) Quantification of cell confluence as a measure of viability in siRNA targeting of VEGF or VEGF+Atg7 (*n*=6). (H) Quantification of cell confluence in KD-HUVECs during autophagy blockade in response to 10 μM chloroquine (*n*=3). For all graphs, error bars indicate the mean±s.d.; **P*<0.05, ***P*<0.005.

Depletion of VEGF increases protein levels of transcription factor FOXO1

Forkhead transcription factors have been linked to autophagy, metabolic regulation and exogenous VEGF signaling (Eijkelenboom and Burgering, 2013). Therefore, perturbation of these pathways prompted us to directly investigate the status and activity of FOXO1 in the absence of VEGF. Increased total FOXO1 protein levels were, indeed, observed in KD-VEGF cells by western blotting (Fig. 5A,B) and immunofluorescence (Fig. 5D–G), although little change was observed in the levels of *Foxo1* transcripts (supplementary material Fig. S3D). Suppression of VEGFR2 signaling by treatment with SU4312 also resulted in an increase of FOXO1 protein levels (Fig. 5C). Transcriptionally active FOXO1 was found translocated to the nucleus, but FOXO1 could also directly contribute to autophagy by cytoplasmic localization (Zhao et al., 2010). We quantified FOXO1 localization in fluorescent images and observed an increase in both nuclear and cytoplasmic localization in KD-VEGF cells, with the larger proportion of FOXO1 observed in the cytoplasm (Fig. 5F,G).

We assessed the transcriptional activity of FOXO1 through evaluation of its target genes by using microarray and RT-PCR analysis. The findings indicate that a subset of direct FOXO1 target genes were increased in KD-VEGF cells, including *Cited2*, *Sod2* and *Sepp1* (supplementary material Fig. S2C). However, other previously reported FOXO1 target genes, such as *Id2* and *Ccnb2*, were not affected in KD-VEGF cells (supplementary material Fig. S3F). This result might indicate a context-dependent FOXO1 transcriptional program or, alternatively, that the contribution of FOXO is cytoplasmic rather than nuclear.

Journal of Cell Science (2015) 128, 2236-2248 doi:10.1242/jcs.163774

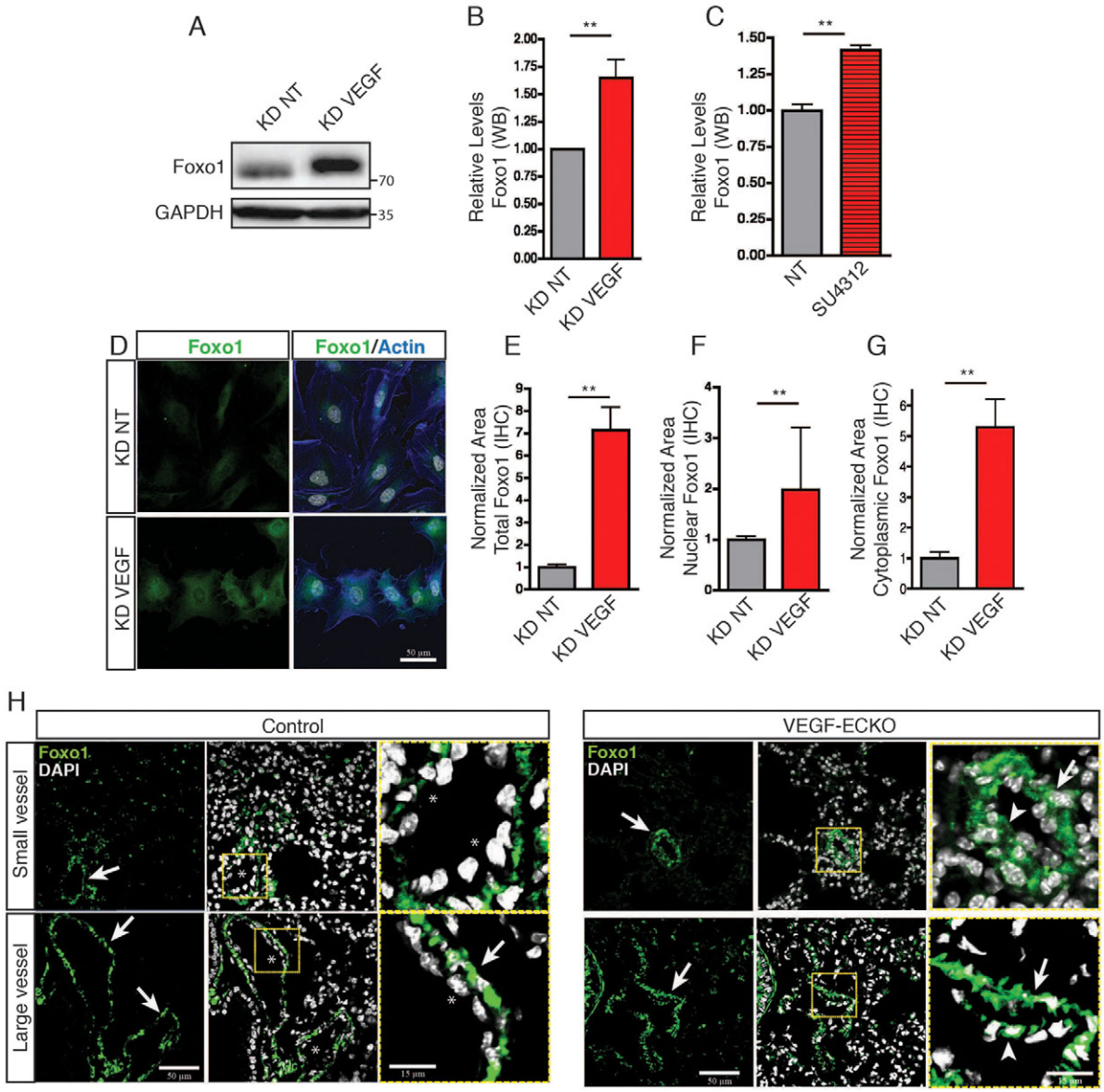

Fig. 5. Activation of FOXO1 is a major consequence of silencing endothelial VEGF. (A) Western blot showing increased FOXO1 protein levels in KD-VEGF cells. (B) Quantification of FOXO1 protein levels (n=10). (C) Increased FOXO1 levels in HUVECs treated with the VEGFR2 inhibitor SU4312 (4 µM) (n=3). (D) Immunodetection of FOXO1 shows increased FOXO1 levels in KD-VEGF HUVECs when compared to control. (E) Quantification of total FOXO1 fluorescence from B (n=3). (F) Quantification of FOXO1 localization in the nucleus (n=3). (G) Quantification of FOXO1 localization to cytoplasm (n=3). For all graphs, error bars indicate ±s.d., *P<0.05; **P<0.005. (H) Increase in endothelial FOXO1 levels in the absence of VEGF *in vivo*. However, FOXO1 is undetected in WT endothelial cells that were evaluated in parallel. Arrowheads denote endothelium positive for FOXO1 in VEGF-ECKO; arrows show FOXO1 expression in smooth muscle cells. Asterisks indicate lack of FOXO1 in the endothelial layer within WT animals.

Because FOXO1 activity and stability is regulated by Akt, JNK and AMPK pathways in other systems, we investigated the status of these pathways in KD-VEGF cells (supplementary material Fig. S4). We were unable to detect any significant changes in these pathways, suggesting that they do not participate in the FOXO1 stability that is observed in the absence of VEGF. FOXO1 is phosphorylated at a comparable rate in KD-NT and KD-VEGF cells (supplementary material Fig. S4D), suggesting that – although overall FOXO1 protein levels are increased – its activation remains stable.

We next investigated the status of FOXO1 in VEGF-ECKO animals that developed in the prolonged absence of autocrine VEGF. Although we found constitutive expression of FOXO1 in the smooth muscle layer surrounding vessels in the lung (Fig. 5H, arrows) of WT mice, the transcription factor was conspicuously absent from the endothelium (Fig. 5H, asterisks). However, in VEGF-ECKO mice, FOXO1 was distinctly expressed in the endothelial layer in addition to its presence in smooth muscle cells (Fig. 5H, arrowheads), again in sharp contrast to WT littermates (Fig. 5H, asterisks).

FOXO1 knockdown rescues mitochondrial deregulation

To identify the transcriptional relationship between FOXO1 and VEGF, expression microarrays were performed on control HUVEC, KD-VEGF and double-knockdown KD-VEGF+FOXO1. We found that expression levels of a subset of genes whose expression was significantly changed under KD-VEGF conditions were restored to wild-type levels in two specific patterns. Expression pattern 1: genes that were upregulated under KD-VEGF conditions and then downregulated under conditions of KD-VEGF+FOXO1

Journal of Cell Science (2015) 128, 2236-2248 doi:10.1242/jcs.163774

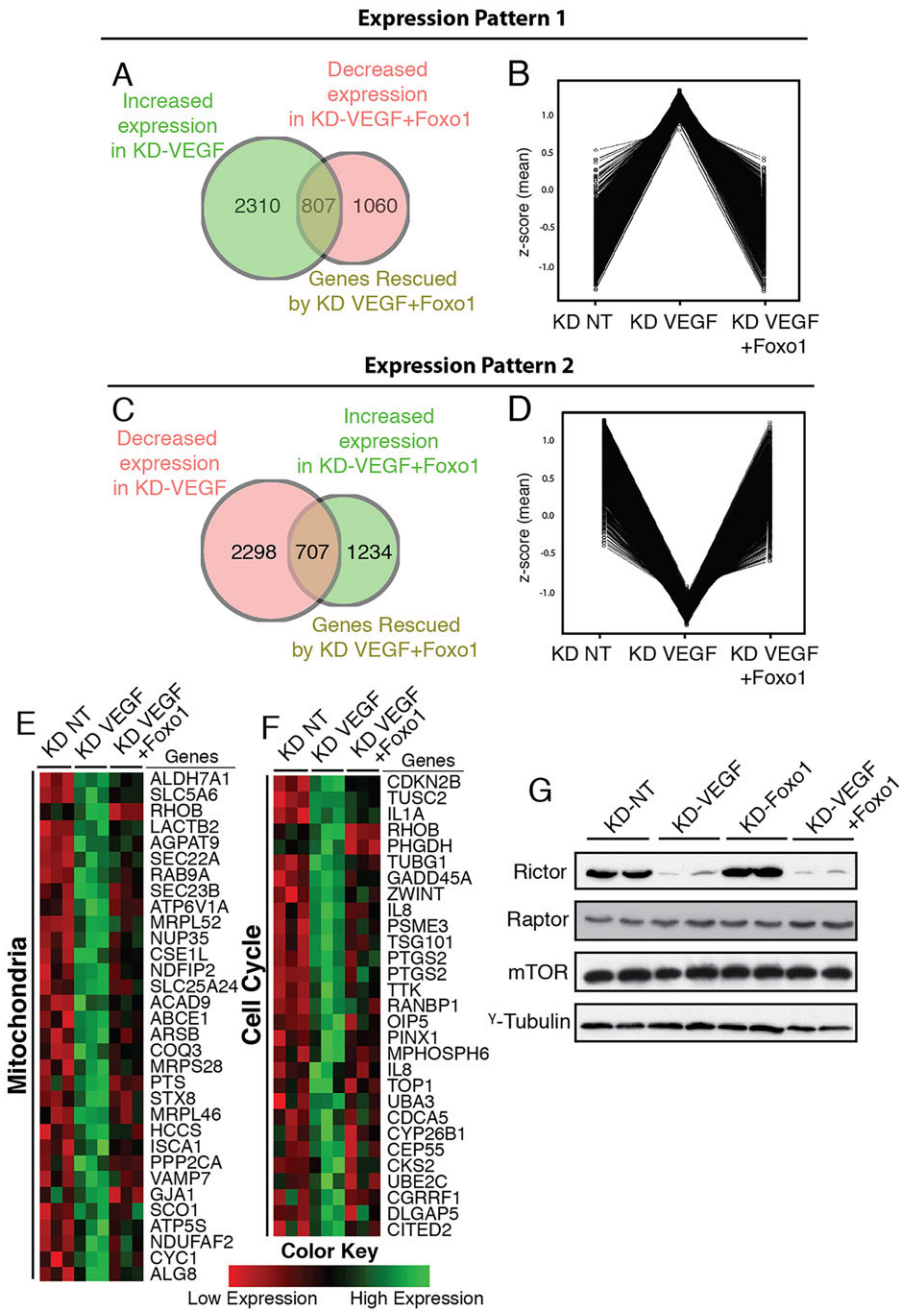

Fig. 6. Knockdown of FOXO1 rescues a subset of deregulated genes but does not rescue changes to the mTOR pathway. *Z* scores of microarray expression values were generated for each gene, and group-statistical means were plotted to assess the trend of changes in expression for KD-VEGF and KD-VEGF+KD-FOXO1 that were rescued compared to controls. Among the probes that were significantly changed between groups, we identified probes with (A,B) increased expression in KD-VEGF and decreased expression in KD-VEGF +KD-FOXO1 (pattern 1), and (C,D) probes with decreased expression in KD-VEGF and increased expression in KD-VEGF+KD-FOXO1 (pattern 2). Significantly rescued genes were subject to DAVID analysis, and heatmaps were generated from two selected GO clusters for (E) mitochondria and (F) cell cycle genes. (G) The effects of KD-FOXO1 rescue on the mTOR pathway were analyzed by western blot probing for Rictor, Raptor and mTOR.

(Fig. 6A,B; supplementary material Table S1) and, expression pattern 2: genes that were downregulated under KD-VEGF conditions and then upregulated under conditions of KD-VEGF+ FOXO1 (Fig. 6C,D; supplementary material Table S2).

To identify cellular functions that are dependent on FOXO1 at transcriptional level, we processed the gene sets comprising expression patterns 1 and 2 by using DAVID analysis. Among many rescued gene clusters (full lists of rescued gene clusters can be found in supplementary material Tables S3,S4), we found rescue of the strongly represented mitochondrial cluster on one hand, as well as a reversal of the expression patterns of cell-cycle gene clusters on the other hand (Fig. 6E,F), which may indicate a reversal of cell cycle arrest and metabolic distress.

Signaling pathways, such as Akt and AMPK, that are typically associated with FOXO1 were found to be unchanged under KD-VEGF conditions (supplementary material Fig. S4). However, further investigation revealed that KD-VEGF had an unexpected effect on the mTOR pathway, in particular a significant reduction in total Rictor protein levels (Fig. 6G). Rictor is one of the crucial components of mTORC2, which have been shown to contribute to the regulation of FOXO1 (Guertin et al., 2006). In fact, siRNA-mediated knockdown of FOXO1 (KD-FOXO1) had no effect on Rictor protein levels, and KD-VEGF+FOXO1 was unable to rescue Rictor protein (Fig. 6G), indicating that Rictor is upstream of FOXO1.

Cell death due to VEGF depletion is rescued by reduction of FOXO1

Because the absence of VEGF in the endothelial compartment induces FOXO1 activity, we assessed whether FOXO1 contributed in any way to the KD-VEGF cellular phenotype. To test this hypothesis, we performed a double knockdown, targeting both

Journal of Cell Science (2015) 128, 2236-2248 doi:10.1242/jcs.163774

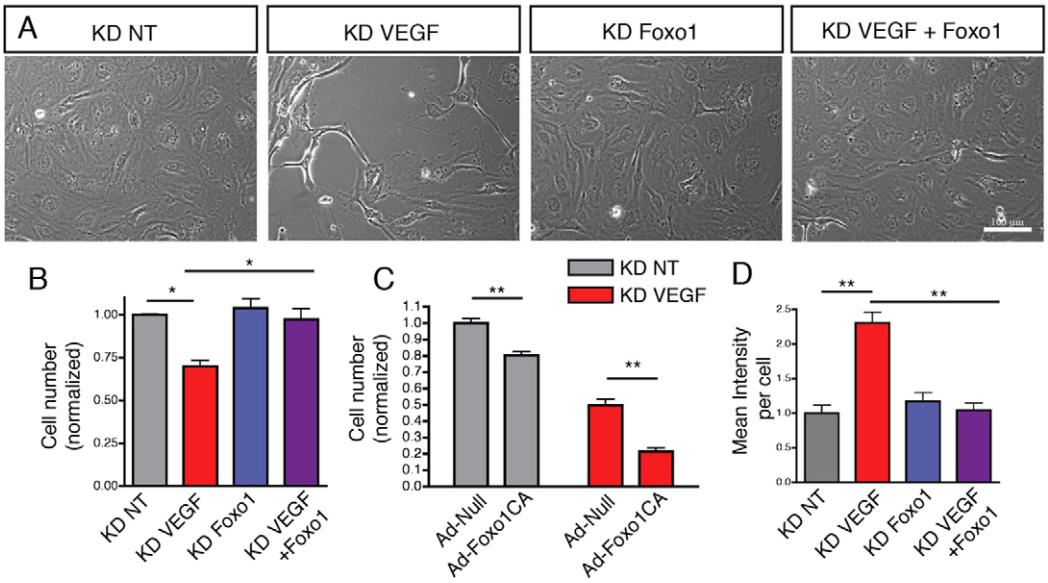

Fig. 7. FOXO1 is essential to trigger cell death and autophagy in the absence of VEGF. (A) Images of endothelial cell cultures under phase contrast show that KD-FOXO1 rescues KD-VEGF-induced cell death (day 4 after first transfection) (scale bar: 100 µm). (B) Quantification of cell number from cultures similar to those shown in A (*n*=3). (C) Constitutively active FOXO1 (Ad-FOXO1CA) reduces cell viability of control and KD-VEGF cells compared to empty vector (Ad-Null, day 5) (*n*=4). (D) Increased autophagic vacuoles were visualized by using the Cyto-ID autophagy detection kit when analyzed by confocal microscopy (*n*=3). For all graphs, error bars indicate mean±s.d.; **P*<0.05, ***P*<0.005.

VEGF and FOXO1 (KD-VEGF+FOXO1) in confluent HUVECs, and assessed cell numbers as a readout for survival (Fig. 7A,B). Depletion of FOXO1, indeed, significantly rescued the cell death observed in KD-VEGF alone (Fig. 7B). Double knockdown of VEGF and FOXO1 did not interfere with VEGF suppression (supplementary material Fig. S3A).

To test whether depletion of FOXO1 increased cell survival in a parallel pathway, we also evaluated single KD-FOXO1 and observed no significant effect compared to the KD-NT condition (Fig. 7B). Interestingly, incorporation of a constitutively active FOXO1 (Ad-FOXO1CA) to KD-NT causes only a modest decrease of approximately 20% in cell survival (Fig. 7C), whereas similar treatment to KD-VEGF results in severe cell death, resulting in approximately 60% cell demise (Fig. 7D), suggesting that FOXO1's activity requires a KD-VEGF background.

Because the microarray and cellular readouts indicate a reversal of the metabolic and cell-death defects seen under KD-VEGF conditions, we next determined whether overactive autophagy was reversed. To assess the role of FOXO1 in KD-VEGF autophagy, we measured autophagic vacuoles under the rescue condition. We found that KD-VEGF/FOXO1 did, indeed, reduce autophagic vacuoles in KD-VEGF to WT levels (Fig. 7D).

DISCUSSION

In this study, we investigated the cellular and signaling functions of autocrine VEGF and, in the process, identified unique features of intracellular VEGF function. We showed that the presence of endothelial VEGF provides integrity to the vasculature in hypoxic conditions *in vivo*, without which intestine, brain and heart are susceptible to vascular lesions and hemorrhages from small vessels. The micro hemorrhages observed in VEGF ECKO mice are likely to be a reflection of focal disruptions of the vasculature due to endothelial cell death, as shown *in vitro*. Importantly, we found that induced deletion of VEGF in the adult endothelium (after WT developmental conditions) causes sudden death in a significant proportion of mutant mice. These results indicate that baseline levels of VEGF in the endothelium are required to support homeostasis of the vasculature. Through a series of microarray analysis, cell signaling and metabolic evaluations, we demonstrated that intracrine VEGF signaling is necessary for endothelial cell survival as KO-VEGF cells can only be rescued by intracellular delivery of VEGF.

At the cellular level, we found that inactivation of VEGF results in mitochondria fragmentation, suppression of cell metabolism, and autophagic cell death. These cellular phenotypes are mediated by FOXO1, which is robustly stabilized in the absence of VEGF. Strikingly, when FOXO1 is removed from VEGF-deficient endothelium, autophagic cell death is rescued, suggesting that the main action of autocrine VEGF is to regulate FOXO1 levels to maintain cellular homeostasis. The effect is likely to be mediated by TORC2, because Rictor is significantly reduced in the absence of intracrine VEGF.

The present study demonstrates that endothelial cell-autonomous VEGF is essential for normal metabolic functions and survival of the endothelium. Our data further indicate that VEGF in the endothelium is required to maintain low FOXO1 protein. In the absence of endogenous VEGF, FOXO1 is increased in the nucleus and cytoplasm, depressing endothelial metabolism and increasing autophagic activity. These findings were further substantiated with transcriptional data that show widespread changes in mitochondrial function and cell cycle that were largely corrected when FOXO1 levels were decreased (readjusted) in KD-VEGF cells. In addition, endothelial cell death in the absence of cell-autonomous VEGF was also rescued through reduction of FOXO1. Overall the data suggest an important biological link between these two pathways in the maintenance of endothelial cell metabolism and survival.

It has been previously shown that exposure of endothelial cultures to VEGF results in deactivation of FOXO1 (Abid et al., 2004), but maintenance of FOXO1 levels through the VEGF pathway was not suspected. FOXO1 is a member of the forkhead family of transcription factors that has been shown to regulate cell cycle progression, reduction of metabolism and response to cell stress

Journal of Cell Science (2015) 128, 2236-2248 doi:10.1242/jcs.163774

(Eijkelenboom and Burgering, 2013). Although high levels of VEGF signaling ultimately leads to FOXO1 degradation, the presence of FOXO1 modulates endothelial responses to VEGF. FOXO1 is, in fact, crucial for proper endothelial signaling cascades in response to VEGF (Zhuang et al., 2013), and contributes to the expression of a set of genes induced by VEGF (Abid et al., 2006). Under homeostatic conditions *in vitro*, FOXO1 regulates a distinct set of vascular angiogenic genes that suppresses the angiogenic response of the endothelium (Potente et al., 2005). *In vivo*, FOXO1-deficient mice die at E11 from vascular defects (Furuyama et al., 2004) and fail to respond properly to treatment with exogenous VEGF. However, a role for this pathway in the maintenance of endothelial cell homeostasis and metabolism in the adult had not been suspected.

Mechanistically, we showed that absence of VEGF results in an increase in total and activated FOXO1. Moreover, we found that the endothelium of VEGF ECKO mice expresses high levels of FOXO1 *in vivo*, indicating an important regulatory loop. Cell demise was rescued in VEGF-ECKO cells by simply decreasing the levels of FOXO1, indicating that this is the main event that triggers cell death downstream of VEGF.

FOXO transcription factors are known to regulate mitochondrial function (Ferber et al., 2012), cell metabolism (Hirota et al., 2008) and autophagy (Zhou et al., 2012; Zhao et al., 2007) in several cell types, but these effects of FOXO have not been clearly linked to VEGF signaling in the endothelium. Only recently, VEGF-mediated activation of cell surface receptors has been associated with suppression of FOXO1 (Zhuang et al., 2013). Our data expand these findings to include a feedback regulatory loop of intracrine VEGF on FOXO1 levels but also raise several additional questions. How does intracrine VEGF regulate FOXO levels? The results presented here suggest mTORC2 to be a likely effector. mTORC2 is one of the two complexes of mTOR, a serine/threonine kinase that controls multiple metabolic processes, such as energy production, protein and lipid synthesis, and responses to cell stress (Zoncu et al., 2011; Bhaskar and Hay, 2007; Laplante and Sabatini, 2012). TORC2 has been shown to regulate FOXO1 (Guertin et al., 2006) and control autophagy (Vlahakis and Powers, 2014). Interestingly, mTORC2 also regulates multiple aspects of mitochondrium physiology (Tan et al., 2014). Thus, Rictor might be the focal point of VEGF deficiency; however, additional experiments are still needed to fully support this thesis.

FOXO1 acts as a main regulator of physiological glucose homeostasis throughout the body and is well known as a target of insulin signaling that suppresses its activity through the PI3K/Akt pathway (Kousteni, 2012). At cellular level, FOXO1 regulates the opposing metabolic processes of glycolysis and glucogenesis (Hirota et al., 2008), and targets a myriad of genes directly involved in metabolic processes, such as PDK4 (Furuyama et al., 2003), glucose-6-phosphatase and phosphoenolpyruvate carboxykinase (van der Vos and Coffer, 2011). In this study, we found that depletion of cell-autonomous VEGF increases FOXO1 activation and suppresses cellular metabolic flux in terms of glycolysis, mitochondrial respiration and fatty acid synthesis.

FOXO transcription factors have been shown to induce autophagy, promoting survival during metabolic stress in hematopoietic stem cells (Warr et al., 2013) and in cardiomyocytes (Hariharan et al., 2010). However, autophagic cell death was also observed as a result of FOXO signaling in pathological settings, such as muscle atrophy (Zhao et al., 2008). Non-canonical (not transcriptional) functions of FOXO1 in autophagy have also been described. In particular, cytoplasmic FOXO1 has been shown to induce autophagic death through direct binding of the autophagic protein Atg7 in cancer cells – a function entirely independent of its DNA-binding ability (Zhao et al., 2010). We observed an increase in both cytoplasmic and nuclear levels of FOXO1 in KD-VEGF cells that allows both direct cytoplasmic pro-autophagy signaling as well as transcriptional effects. In our studies, FOXO1 suppressed the autophagic phenotype exhibited by KO-VEGF cells but, constitutively active FOXO1 alone, does not cause cell demise. Therefore, VEGF promoted additional changes in the biology of the endothelium that sensitized the endothelium to alterations in FOXO1 levels.

It should be stressed, however, that our findings strongly suggest alternative effects of VEGF in targets other than FOXO1. In fact, our transcriptional data indicate that other genes are deregulated upon VEGF decrease, and some of these were not rescued by a decrease of FOXO1. Furthermore, as previously discussed, although a reduction in FOXO1 rescues VEGF depletion, we are unable to induce cell death to the same degree as observed in VEGF-null endothelium. This indicates that VEGF alters additional pathways that control survival, and that FOXO1 is a crucial trigger, but only in the context of a previously sensitized endothelium. The effects of VEGF-depletion in mitochondrium fragmentation might be such a 'sensitized' condition.

Overall, the findings presented here indicate that cell-autonomous VEGF is required for the regulation of endothelial cell metabolism and autophagy in fully differentiated cells. This function adds to the long list of contributions of this signaling pathway to endothelial biology and provides a call to caution to pharmacological treatments that promote long-term suppression to the VEGF signaling pathway.

MATERIALS AND METHODS

Materials

In all cases, human VEGF isoform 165 (hVEGF165; simply referred to in the text as VEGF) was used. hVEGF165 and the B20 anti-VEGF antibody (Liang et al., 2006) were provided by the NIH Repository, Genentech (San Francisco, CA) and used as rVEGF at 100 ng/ml unless otherwise indicated. Antibodies against human VEGFR2, phosphorylated VEGFR2 at residue Tyr1175, cleaved and whole caspase 3, GAPDH, FOXO1 and Rictor were from Cell Signaling. Antibodies against γ-tubulin and SU4312 were obtained from Sigma-Aldrich. Cell viability was determined by using cell counting kit-8 (CCK-8 kit, Dojindo Molecular Technologies) as described previously (Lee et al., 2007). The Cyto-ID Autophagy detection kit was used to label autophagic vesicles (Enzo Life Sciences).

Generation of mice and cre induction

Generation of floxed-VEGF (Gerber et al., 1999) and inducible VE-cadherin-Cre (VE-Cad-iCre) mice have been previously described (Monvoisin et al., 2006). These mouse lines were interbred to produce homozygous floxed-VEGF/VE-Cad-iCre mice that were induced to excise endothelial VEGF following treatment with tamoxifen. Tamoxifen was administered for 6 days by daily gavage and injections starting at 10 weeks of age and mice were monitored for lethality.

Hypoxia treatment of mice

Prior to treatment, mice were housed in standard polypropylene cages in a room maintained at 25°C, and allowed full access to food and water. All animals were housed in a pathogen-free environment within an AAALAC-approved vivarium at UCLA, and experiments were performed in accordance with the guidelines of the Committee for Animal Research.

The mice were randomly assigned to one of the experimental groups per genotype: (1) control group (ten Cre-negative mice and seven Cre-positive mice) maintained under normoxic conditions; (2) experimental group (15 Cre negative mice and 15 Cre positive mice) exposed to hypoxia for 1 week followed by normoxia for 2 weeks and additional hypoxia for 2 weeks. Humidity in the chamber was maintained at 40–50% and temperature at

22–24°C. All groups were induced in custom-built chambers (Oxycycler model X, Biospherix, Redfield, NY) connected to a supply of O_2 and N_2. A computer was programmed to maintain the partial pressure (tension) of oxygen (pO_2) at 8%. The intermittent hypoxia procedure used in the study reduced oxygen saturation by 60%. For the treatment, the pO_2 gradually decreased to reach the target level. After exposing the animals to the decreased pO_2 for 1 week, the pO_2 was gradually increased to reach the normal level in about 4 h. The chambers were cleaned daily. For the normoxic control, animals were kept in the chamber circulated with room air for the identical corresponding period.

Cell culture

Human umbilical vein endothelial cells (HUVECs; VEC Technologies), human dermal microvascular endothelial cells (HDMEC; gift of Joyce Bischoff), and hemangioma endothelial cells (HemECs; gift of Joyce Bischoff) were cultured in complete MCDB131 medium (VEC Technologies). Primary endometrial epithelial cells (Endo. Epithel), Human umbilical mesenchymal stem cells (HUMSC) and myofibroblasts were cultured in DMEM with 10% FBS. Primary mouse endothelial cells were isolated from adult VEGF-ECKO as described previously (Lee et al., 2007). IMECs were derived from homozygous flox-flox VEGF mice crossed with mice of the Immortomouse line (Charles River Labs) and harvested from the lung as previously described (He et al., 2012). Floxed-VEGF was excised by adenoviral delivery of Cre protein as described previously (Chen et al., 2010), and then checked for complete excision by genomic PCR. IMECs were cultured under immortalized conditions in DMEM supplemented with 100 U interferon-γ at 33°C. After expansion, IMECs were cultured under standard conditions (37°C in MCDB131 with 10% FBS) to inactivate the immortalization promoter, passaged one to four times and used for experiments.

VEGF ELISA

Human VEGF Quantikine ELISA kits (R&D Systems) were used to assess VEGF in the lysate and medium of confluent cells in 6-well plates. Confluent cells were incubated with 0.65 ml for 24 h, then this medium was collected and the remaining cell layer was lysed with 0.15 ml RIPA buffer [50 mM Tris pH 7.4, 150 mM NaCl, 1% NP-40, 0.25% sodium deoxycholate, 1 mM EDTA, 1 mM sodium orthovanadate, 10 mM glycerophosphate, and protease inhibitors 1 mM phenyl-methanesulfonylfluoride (PMSF), complete EDTA-free protease inhibitor tablet (Roche)]. Cell lysates were scraped into tubes, incubated under agitation at 4°C for 30 min, then centrifuged at 20,000 ***g*** for 20 min at 4°C. Total medium and lysate samples were loaded onto the ELISA as per manufacturer's instructions, and the total amount of VEGF in pg per well was calculated from VEGF pg/ml values.

Incucyte live cell imaging

For cell death assays, IMECs were grown to confluence in 96-well plates then treated with 0.1 µM YOYO-1 (Essen Bioscience) in serum-free medium as per the manufacturer's instructions, with images collected every 2 h. Thresholds were set so that a single fluorescent nuclei was counted as an 'object' band, cell death events were estimated by percent coverage of the confluent plate or 'object confluence', as extrapolated by the Essen Bioscience software. The mean of the data was calculated and plotted by using Essen Incucyte software.

Transfection of siRNA

Confluent HUVECs were transfected twice (on days 1 and 3) with 20 nmol of siRNA oligonucleotides by using siPORT amine transfection reagent (catalog number AM4503; Ambion) in serum-free medium (optiMEM I; Invitrogen). Cells were analyzed by western blotting, RT-PCR, microarray or for cell count on day 5 unless otherwise indicated. Oligonucleotides used: siGENOME human VEGFA (7422) siRNA, ON-TARGETplus human FOXO1 (2308) siRNA – SMARTpool, ON-TARGETplus non-targeting siRNA #1 (KD-NT) (Thermo Scientific).

Real-time reverse transcriptase (RT)-PCR

RNA was isolated and amplified as described previously (He et al., 2012). Primers used: VEGFA: Hs00900055_m1, FOXO1: Hs01054576_m1, CITED2: Hs01897804_m1, FOXO1: Hs01054576_m1, FOXO3: Hs00921424_m1, FOXO4: Hs00172973_m1, CCNB2: Hs00270424_m1, SOD2: Hs00167309_m1, SPRY2: Hs01921749_s1, KDR: Hs00911700_m1, CITED2: Hs01897804_m1, CCND1:Hs00765553_m1, MMP7: Hs01042796_m1, SEPP1: Hs01032845_m1, DCN: Hs00370384_m1, ID2: Hs04187239_m1 (Applied Biosystems). Primers used to verify microarray: CCL23 5′-ctcctacaccccacgaagcat-3′, 5′-ttcttcctggtcttgatccgt-3′ (Kim et al., 2011); NDRG4 5′-ggccttctgcatgtagtgatccg-3′, 5′-ggtgatctcctgcatgtcctcg-3′ (Ding et al., 2012); ESM1 5′-aaggctgctgatgtagttc-3′, 5′-gctatttatggaagtgta-tgtgttt-3′ (Kim et al., 2012); TAGLN 5′-aagaatgatgggcactaccg-3′, 5′-actg-atgatctgccgaggtc-3′ (Chen et al., 2011).

Viral transduction

Cells were infected overnight with Lentiviral-VEGF164 or control Lentiviral-YFP at a p24 titer of 0.16 µg in serum-free medium with protamine sulfate (4 µg/ml). Adenoviral infection was performed as described previously (Chen et al., 2010).

Western blots

Endothelial cells were preincubated for 5 min with 100 µM Na_3VO_4 to inhibit phosphatase activity and then harvested for total protein in RIPA buffer as for the 'VEGF ELISA'. Equivalent levels of protein, determined using the DC protein assay reagent (Bio-Rad Laboratories) were separated by SDS-PAGE, transferred to nitrocellulose membranes (Bio-Rad), probed with indicated antibodies, detected by Supersignal West Pico Chemiluminescent Substrate (Pierce Biotechnology), and quantified by densitometry using Image Lab.

Metabolic measurements

Glucose consumption and lactate production were measured using the Bioanalyzer 4 (Nova Biomedical). Cells were seeded at 150,000 cells per well in triplicate. Fresh medium with or without 10% FBS was added to the wells 24 h after seeding, and glucose depletion from and lactate addition to the culture medium over the following 24 h period were determined. Values were normalized to cell numbers and time intervals.

Basal oxygen consumption rates and mitochondrial respiratory capacity were measured using the XF24 Extracellular Flux Analyzer (Seahorse Bioscience). Cells were seeded at 62,500 cells per well in a 24-well plate 48 h prior to assay, and medium with or without 10% FBS was renewed 24 h prior to assay. Values were normalized to total the protein content using the BCA Protein Assay Kit (Pierce). Triglyceride synthesis was measured as previously described (Castellani et al., 2008).

Microarray analysis

Illumina gene expression data were normalized using the quintile normalization method. Normalization and quality control were performed by using the 'lima' iR package (Smyth, 2005). We filtered out noise range probes by requiring that probes have at least two significant ($P<0.05$) detections within the triplicates of at least one experiment group. This resulted in retaining 20,003 probes out of 47,217 for the inferential analysis. Empirical Bayes moderated *t*-tests (Smyth, 2004) were performed to compare expression between genes expressed in control and KD-VEGF cells. *Z* scores of expression values were generated for each gene, and group means were plotted.

DAVID analysis was performed only on genes showing significantly different expression ($P<0.05$) with log-fold changes >1 between KD-NT and KD-VEGF to create 'upregulated' GO clusters. Similarly, DAVID analysis was performed on genes showing significantly different expression with log-fold changes <1 to create 'downregulated' GO clusters.

To pick gene clusters that fit expression pattern 1, DAVID analysis was performed on the set of genes that were significantly upregulated in KD-VEGF compared to control, and significantly downregulated in KD-VEGF+FOXO1 compared to KD-VEGF. The list of genes that fit pattern 2 was created using the opposite expression patterns. DAVID analysis was performed on these lists of genes and GO clusters were made into heat-maps using *z*-scores of expression values.

Statistical analysis

Differences between groups were evaluated using one-way ANOVA followed with Tukey's post-hoc multiple comparison test. Selected

biologically interesting *P*-values are reported. Data pairs were compared by using two-tailed Student's *t*-test. Survival curves were constructed using the Kaplan–Meier method and were compared between groups with the log rank test. All analyses were performed using Prism (v4.0c; GraphPad Software) unless otherwise indicated. *P*-values of <0.05 were considered significant.

Immunocytochemistry and confocal microscopy

Endothelial cells were grown to confluence on coverslips in 6-well plates and transfected as above.

For autophagy, wells were treated with Green Autophagy Detection reagent and Hoechst 33342 nuclear stain (Cyto-ID Autophagy detection kit; Enzo Life Sciences) for 30 min at 37°C. The cells were then washed and fixed in 3% PFA for 15 min. For FOXO1 and Hsp60 cell staining, cells grown on coverslips were fixed for 15 min in 3% PFA. The coverslips were incubated overnight in polyclonal anti-FOXO1 or anti-Hsp60 antibody followed by incubation with anti-rabbit Alexa Fluor®488 for 1 h. Nuclei were counterstained with DAPI.

For staining in histological sections, adult lungs were fixed overnight in 2% PFA and embedded in paraffin. Antigen retrieval was achieved by a combination of proteinase K treatment and Tris-EDTA epitope retrieval. Sections were incubated overnight in polyclonal anti-FOXO1 antibody followed by HRP-conjugated anti-rabbit for 1 h. Signal amplification was achieved by using Molecular Probes® TSATM Kit, catalog number 22. Nuclei were counterstained with DAPI.

All slides were mounted in Mowiol®4-88. Carl Zeiss LSM 510 META Laser Confocal Microscope was used to acquire 40× images with 0.80 aperture at room temperature. ZEN®-2009 was used as the acquisition software. Exported files were quantified using ImageJ®. *P*-values were obtained in a Student's *t*-test from the average percent area, normalized to WT samples.

Acknowledgements

We thank the Tissue Procurement Core Laboratory Shared Resource at UCLA and the UCLA Vector Core. The UCLA Vector Core is supported by JCCC/P30 CA016042 and CURE/P30 DK041301.

Competing interests

The authors declare no competing or financial interests.

Author contributions

C.K.D. designed and performed experiments, analyzed data and wrote the paper. C.M.W. designed and performed experiments, analyzed data and assisted in manuscript preparation. K.H., A.K., A.X.T.-C., L.W.C., V.A. and S.Z. performed experiments. L.D. and D.E. performed all the microarray analysis and assisted in the GO evaluations. H.R.C., A.M.vdB. and M.P. provided crucial reagents and guidance. M.L.I.-A. designed the study and wrote the paper.

Funding

This study was supported by funds from the National Institutes of Health (NIH) Research Project Grant Program [grant numbers R01 CA126935 to M.L.I.-A. and T32 NIH T32 HL69766 to C.K.D.]. Deposited in PMC for release after 12 months.

Supplementary material

Supplementary material available online at
http://jcs.biologists.org/lookup/suppl/doi:10.1242/jcs.163774/-/DC1

References

Abid, M. R., Guo, S., Minami, T., Spokes, K. C., Ueki, K., Skurk, C., Walsh, K. and Aird, W. C. (2004). Vascular endothelial growth factor activates PI3K/Akt/Forkhead signaling in endothelial cells. *Arterioscler. Thromb. Vasc. Biol.* **24**, 294-300.

Abid, M. R., Shih, S.-C., Otu, H. H., Spokes, K. C., Okada, Y., Curiel, D. T., Minami, T. and Aird, W. C. (2006). A novel class of vascular endothelial growth factor-responsive genes that require forkhead activity for expression. *J. Biol. Chem.* **281**, 35544-35553.

Bhaskar, P. T. and Hay, N. (2007). The two TORCs and Akt. *Dev. Cell* **12**, 487-502.

Carmeliet, P., Ferreira, V., Breier, G., Pollefeyt, S., Kieckens, L., Gertsenstein, M., Fahrig, M., Vandenhoeck, A., Harpal, K., Eberhardt, C. et al. (1996). Abnormal blood vessel development and lethality in embryos lacking a single VEGF allele. *Nature* **380**, 435-439.

Cartron, P.-F., Petit, E., Bellot, G., Oliver, L. and Vallette, F. M. (2014). Metaxins 1 and 2, two proteins of the mitochondrial protein sorting and assembly machinery, are essential for Bak activation during TNF alpha triggered apoptosis. *Cell. Signal.* **26**, 1928-1934.

Castellani, L. W., Nguyen, C. N., Charugundla, S., Weinstein, M. M., Doan, C. X., Blaner, W. S., Wongsiriroj, N. and Lusis, A. J. (2008). Apolipoprotein AII is a regulator of very low density lipoprotein metabolism and insulin resistance. *J. Biol. Chem.* **283**, 11633-11644.

Chen, D., Zhang, X.-Y. and Shi, Y. (2006). Identification and functional characterization of hCLS1, a human cardiolipin synthase localized in mitochondria. *Biochem. J.* **398**, 169-176.

Chen, T. T., Luque, A., Lee, S., Anderson, S. M., Segura, T. and Iruela-Arispe, M. L. (2010). Anchorage of VEGF to the extracellular matrix conveys differential signaling responses to endothelial cells. *J. Cell Biol.* **188**, 595-609.

Chen, R., Feng, C. and Xu, Y. (2011). Cyclin-dependent kinase-associated protein Cks2 is associated with bladder cancer progression. *J. Int. Med. Res.* **39**, 533-540.

dela Paz, N. G., Walshe, T. E., Leach, L. L., Saint-Geniez, M. and D'Amore, P. A. (2012). Role of shear-stress-induced VEGF expression in endothelial cell survival. *J. Cell Sci.* **125**, 831-843.

Ding, W., Zhang, J., Yoon, J.-G., Shi, D., Foltz, G. and Lin, B. (2012). NDRG4 is downregulated in glioblastoma and inhibits cell proliferation. *OMICS* **16**, 263-267.

Eijkelenboom, A. and Burgering, B. M. T. (2013). FOXOs: signalling integrators for homeostasis maintenance. *Nat. Rev. Mol. Cell Biol.* **14**, 83-97.

Fan, J., Ponferrada, V. G., Sato, T., Vemaraju, S., Fruttiger, M., Gerhardt, H., Ferrara, N. and Lang, R. A. (2014). Crim1 maintains retinal vascular stability during development by regulating endothelial cell Vegfa autocrine signaling. *Development* **141**, 448-459.

Ferber, E. C., Peck, B., Delpuech, O., Bell, G. P., East, P. and Schulze, A. (2012). FOXO3a regulates reactive oxygen metabolism by inhibiting mitochondrial gene expression. *Cell Death Differ.* **19**, 968-979.

Ferrara, N., Carver-Moore, K., Chen, H., Dowd, M., Lu, L., O'Shea, K. S., Powell-Braxton, L., Hillan, K. J. and Moore, M. W. (1996). Heterozygous embryonic lethality induced by targeted inactivation of the VEGF gene. *Nature* **380**, 439-442.

Franco, M., Roswall, P., Cortez, E., Hanahan, D. and Pietras, K. (2011). Pericytes promote endothelial cell survival through induction of autocrine VEGF-A signaling and Bcl-w expression. *Blood* **118**, 2906-2917.

Furuyama, T., Kitayama, K., Yamashita, H. and Mori, N. (2003). Forkhead transcription factor FOXO1 (FKHR)-dependent induction of PDK4 gene expression in skeletal muscle during energy deprivation. *Biochem. J.* **375**, 365-371.

Furuyama, T., Kitayama, K., Shimoda, Y., Ogawa, M., Sone, K., Yoshida-Araki, K., Hisatsune, H., Nishikawa, S.-i., Nakayama, K., Nakayama, K. et al. (2004). Abnormal angiogenesis in FOXO1 (Fkhr)-deficient mice. *J. Biol. Chem.* **279**, 34741-34749.

Gerber, H. P., Hillan, K. J., Ryan, A. M., Kowalski, J., Keller, G. A., Rangell, L., Wright, B. D., Radtke, F., Aguet, M. and Ferrara, N. (1999). VEGF is required for growth and survival in neonatal mice. *Development* **126**, 1149-1159.

Gerber, H.-P., Malik, A. K., Solar, G. P., Sherman, D., Liang, X. H., Meng, G., Hong, K., Marsters, J. C. and Ferrara, N. (2002). VEGF regulates haematopoietic stem cell survival by an internal autocrine loop mechanism. *Nature* **417**, 954-958.

Guertin, D. A., Stevens, D. M., Thoreen, C. C., Burds, A. A., Kalaany, N. Y., Moffat, J., Brown, M., Fitzgerald, K. J. and Sabatini, D. M. (2006). Ablation in mice of the mTORC components raptor, rictor, or mLST8 reveals that mTORC2 is required for signaling to Akt-FOXO and PKCalpha, but not S6K1. *Dev. Cell* **11**, 859-871.

Hariharan, N., Maejima, Y., Nakae, J., Paik, J., DePinho, R. A. and Sadoshima, J. (2010). Deacetylation of FOXO by Sirt1 plays an essential role in mediating starvation-induced autophagy in cardiac myocytes. *Circ. Res.* **107**, 1470-1482.

He, H., Xu, J., Warren, C. M., Duan, D., Li, X., Wu, L. and Iruela-Arispe, M. L. (2012). Endothelial cells provide an instructive niche for the differentiation and functional polarization of M2-like macrophages. *Blood* **120**, 3152-3162.

Hirota, K., Sakamaki, J.-I., Ishida, J., Shimamoto, Y., Nishihara, S., Kodama, N., Ohta, K., Yamamoto, M., Tanimoto, K. and Fukamizu, A. (2008). A combination of HNF-4 and FOXO1 is required for reciprocal transcriptional regulation of glucokinase and glucose-6-phosphatase genes in response to fasting and feeding. *J. Biol. Chem.* **283**, 32432-32441.

Kim, C.-S., Kang, J.-H., Cho, H.-R., Blankenship, T. N., Erickson, K. L., Kawada, T. and Yu, R. (2011). Potential involvement of CCL23 in atherosclerotic lesion formation/progression by the enhancement of chemotaxis, adhesion molecule expression, and MMP-2 release from monocytes. *Inflamm. Res.* **60**, 889-895.

Kim, J. H., Park, M. Y., Kim, C. N., Kim, K. H., Kang, H. B., Kim, K. D. and Kim, J. W. (2012). Expression of endothelial cell-specific molecule-1 regulated by hypoxia inducible factor-1α(in human colon carcinoma: impact of ESM-1 on prognosis and its correlation with clinicopathological features. *Oncol. Rep.* **28**, 1701-1708.

Kousteni, S. (2012). FOXO1, the transcriptional chief of staff of energy metabolism. *Bone* **50**, 437-443.

Laplante, M. and Sabatini, D. M. (2012). mTOR signaling in growth control and disease. *Cell* **149**, 274-293.

Lee, S., Chen, T. T., Barber, C. L., Jordan, M. C., Murdock, J., Desai, S., Ferrara, N., Nagy, A., Roos, K. P. and Iruela-Arispe, M. L. (2007). Autocrine VEGF signaling is required for vascular homeostasis. *Cell* **130**, 691-703.

Liang, W.-C., Wu, X., Peale, F. V., Lee, C. V., Meng, Y. G., Gutierrez, J., Fu, L., Malik, A. K., Gerber, H.-P., Ferrara, N. et al. (2006). Cross-species vascular endothelial growth factor (VEGF)-blocking antibodies completely inhibit the growth of human tumor xenografts and measure the contribution of stromal VEGF. *J. Biol. Chem.* **281**, 951-961.

Lichtenberger, B. M., Tan, P. K., Niederleithner, H., Ferrara, N., Petzelbauer, P. and Sibilia, M. (2010). Autocrine VEGF signaling synergizes with EGFR in tumor cells to promote epithelial cancer development. *Cell* **140**, 268-279.

Maharaj, A. S. R., Saint-Geniez, M., Maldonado, A. E. and D'Amore, P. A. (2006). Vascular endothelial growth factor localization in the adult. *Am. J. Pathol.* **168**, 639-648.

Matsumoto, T. and Claesson-Welsh, L. (2001). VEGF receptor signal transduction. *Sci. STKE* **2001**, re21.

Mizushima, N., Yoshimori, T. and Levine, B. (2010). Methods in mammalian autophagy research. *Cell* **140**, 313-326.

Monvoisin, A., Alva, J. A., Hofmann, J. J., Zovein, A. C., Lane, T. F. and Iruela-Arispe, M. L. (2006). VE-cadherin-CreER T2 transgenic mouse: a model for inducible recombination in the endothelium. *Dev. Dyn.* **235**, 3413-3422.

Namiki, A., Brogi, E., Kearney, M., Kim, E. A., Wu, T., Couffinhal, T., Varticovski, L. and Isner, J. M. (1995). Hypoxia induces vascular endothelial growth factor in cultured human endothelial cells. *J. Biol. Chem.* **270**, 31189-31195.

Potente, M., Urbich, C., Sasaki, K.-I., Hofmann, W. K., Heeschen, C., Aicher, A., Kollipara, R., DePinho, R. A., Zeiher, A. M. and Dimmeler, S. (2005). Involvement of FOXO transcription factors in angiogenesis and postnatal neovascularization. *J. Clin. Invest.* **115**, 2382-2392.

Potting, C., Tatsuta, T., König, T., Haag, M., Wai, T., Aaltonen, M. J. and Langer, T. (2013). TRIAP1/PRELI complexes prevent apoptosis by mediating intramitochondrial transport of phosphatidic acid. *Cell Metab.* **18**, 287-295.

Samuel, S., Fan, F., Dang, L. H., Xia, L., Gaur, P. and Ellis, L. M. (2010). Intracrine vascular endothelial growth factor signaling in survival and chemoresistance of human colorectal cancer cells. *Oncogene* **30**, 1205-1212.

Smyth, G. K. (2004). Linear models and empirical bayes methods for assessing differential expression in microarray experiments. *Stat. Appl. Genet. Mol. Biol.* **3**, Article3.

Smyth, G. K. (2005). limma: Linear Models Microarray Data. In *Bioinformatics and Computational Biology Solutions using R and Bioconductor:* Statistics for Biology and Health (ed. R. Gentleman, V. Carey, W. Huber, R. Irizarry and S. Dudoit). pp. 397-420. New York: Springer.

Tan, S.-H., Shui, G., Zhou, J., Shi, Y., Huang, J., Xia, D., Wenk, M. R. and Shen, H.-M. (2014). Critical role of SCD1 in autophagy regulation via lipogenesis and lipid rafts-coupled AKT-FOXO1 signaling pathway. *Autophagy* **10**, 226-242.

van der Vos, K. E. and Coffer, P. J. (2011). The extending network of FOXO transcriptional target genes. *Antioxid. Redox Signal.* **14**, 579-592.

Vlahakis, A. and Powers, T. (2014). A role for TOR complex 2 signaling in promoting autophagy. *Autophagy* **10**, 2085-2086.

Warr, M. R., Binnewies, M., Flach, J., Reynaud, D., Garg, T., Malhotra, R., Debnath, J. and Passegué, E. (2013). FOXO3A directs a protective autophagy program in haematopoietic stem cells. *Nature* **494**, 323-327.

Zhao, J., Brault, J. J., Schild, A., Cao, P., Sandri, M., Schiaffino, S., Lecker, S. H. and Goldberg, A. L. (2007). FOXO3 coordinately activates protein degradation by the autophagic/lysosomal and proteasomal pathways in atrophying muscle cells. *Cell Metab.* **6**, 472-483.

Zhao, J., Brault, J. J., Schild, A. and Goldberg, A. L. (2008). Coordinate activation of autophagy and the proteasome pathway by FOXO transcription factor. *Autophagy* **4**, 378-380.

Zhao, Y., Yang, J., Liao, W., Liu, X., Zhang, H., Wang, S., Wang, D., Feng, J., Yu, L. and Zhu, W.-G. (2010). Cytosolic FOXO1 is essential for the induction of autophagy and tumour suppressor activity. *Nature* **12**, 665-675.

Zhou, J., Liao, W., Yang, J., Ma, K., Li, X., Wang, Y., Wang, D., Wang, L., Zhang, Y., Yin, Y. et al. (2012). FOXO3 induces FOXO1-dependent autophagy by activating the AKT1 signaling pathway. *Autophagy* **8**, 1712-1723.

Zhuang, G., Yu, K., Jiang, Z., Chung, A., Yao, J., Ha, C., Toy, K., Soriano, R., Haley, B., Blackwood, E. et al. (2013). Phosphoproteomic analysis implicates the mTORC2-FOXO1 axis in VEGF signaling and feedback activation of receptor tyrosine kinases. *Sci. Signal.* **6**, ra25.

Zoncu, R., Efeyan, A. and Sabatini, D. M. (2011). mTOR: from growth signal integration to cancer, diabetes and ageing. *Nat. Rev. Mol. Cell Biol.* **12**, 21-35.

Supplemental Figures and Tables Summary

Figure S1 shows a lack of apoptosis by several methods: western blots detecting cleaved-Caspase 3 and cleaved-PARP, and TUNEL staining for nicked DNA. Figure S2 shows representative gene clusters from DAVID analysis of genes down-regulated in KD-VEGF (blood vessel, Golgi) as well as a "Foxo1 target" cluster assembled from the literature. Figure S3 shows microarray validation and changes in Foxo1 target genes in KD-VEGF conditions by RT-PCR. Figure S4 investigates possible upstream signaling pathways that may contribute to Foxo1 stability. Table S1 and S2 provide a detailed list of the top ontological clusters derived from the list of genes most changed between KD-VEGF and KD-NT HUVECs in an RNA microarray. Table S3 and S4 provide the top clusters derived from the list of genes responding to Foxo1 rescue following "Expression Pattern 1" (Table S3) and "Expression Pattern 2" (Table S4).

Supplemental Figure 1. Apoptosis was not detected in KD-VEGF HUVECs. (A) Total and cleaved Caspase 3 were detected by western blot in 25ug of protein lysate from KD-VEGF and KD-NT HUVECs. (B) Total and cleaved PARP were analyzed as above. Positive and negative apoptosis controls were provided by non-treated and staurosporine (1hr 1μM) treated HUVECs. (C) TUNEL staining was performed on KD-VEGF and KD-NT cells. Out of approximately 50,000 cells, 4 were found to be TUNEL positive in the KD-VEGF condition, while none were TUNEL positive in KD-NT. Nuclease treatment was used to create nicked DNA as a positive control. Error bars mean +/- SD, *, $P<0.05$; **, $P<0.005$

Supplemental Figure 2. Autocrine VEGF is required to maintain endothelial identity, mitochondrial and Golgi transcriptome. HUVECs were transfected with siRNA targeting VEGF and total RNA was isolated on day 4 after first transfection (n=3). Gene expression profile was assessed with Illumina human gene chip expression assay. GO clusters extracted from genes significantly up- and down-regulated in KD-VEGF analyzed by DAVID. Heatmaps highlight a subset of two down-regulated GO clusters: (A) blood vessel and (B) Golgi. (C) Select Foxo1 targets significantly up- or down-regulated.

Supplemental Figure 3. Microarray validation and further analysis of Foxo1 target genes (A) A significant decrease in VEGF levels was maintained in double-knockdown conditions. Two of the top genes found (B) increased (CCL23 and NDRG4) and (C) decreased (ESM1 and TAGLN) in the KD-VEGF condition of the microarray were validated by RT-PCR. (D) RT-PCR analysis of several genes of interest showed that decrease in VEGF levels was maintained over several days, Foxo1 levels remained largely unchanged, and VEGFR-2 levels were drastically increased. Several previously-described Foxo1 targets were found to be (E) increased as expected in the KD-VEGF condition by RT-PCR (CITED2, SOD2, SEPP1) or (F) found to be unchanged or regulated contrary to previous reports (SPRY2, MMP7, DCN, ID2, CCND1, CCNB2). Error bars mean +/- SD, *, $P<0.05$; **, $P<0.005$

Supplemental Figure 4. No changes observed in signaling pathways upstream of Foxo1 or in phospho-Foxo1 levels. Western blots investigating the phospo- activation status of (A) Akt, (B) JNK and (C) AMPK were performed, revealing no significant differences between KD-VEGF and KD-NT conditions. (D) Western blots were performed and quantified showing phospho-Foxo1 status was unchanged relative to total Foxo1 protein in KD-NT and KD-VEGF HUVECs.

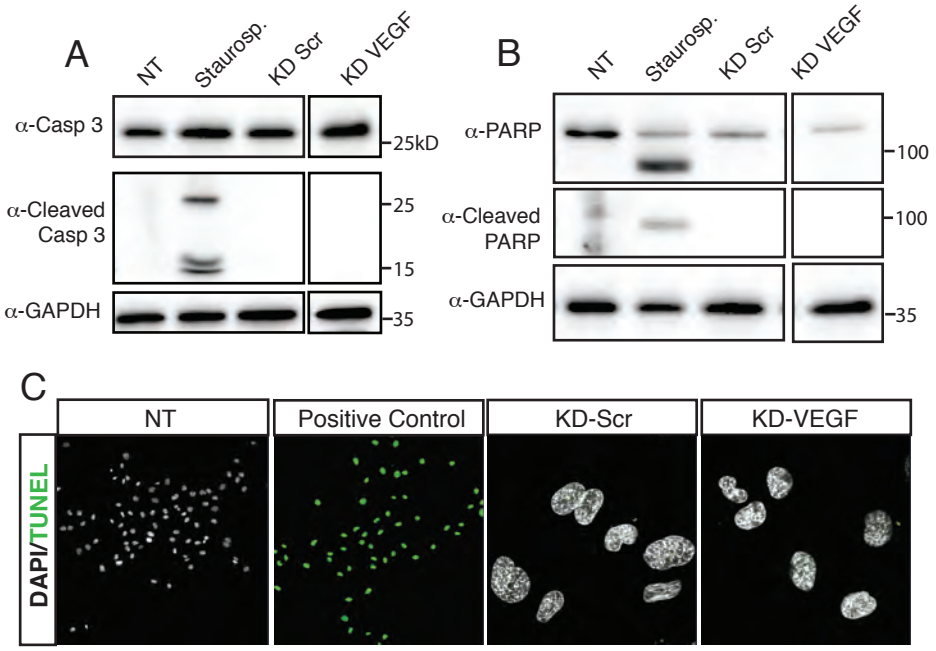

Supplemental Figure 1: Apoptosis was not detected in KD-VEGF HUVECs

(A) Total and cleaved Caspase 3 were detected by western blot in 25ug of protein lysate from KD-VEGF and KD-Scr HUVECs. (B) Total and cleaved PARP were analyzed as above. Positive and negative apoptosis controls were provided by non-treated and staurosporine (1hr 1uM) treated HUVECs. (C) TUNEL staining was performed on KD-VEGF and KD-Scr cells. Out of approximately 50,000 cells, 4 were found to be TUNEL positive in the KD-VEGF condition, while none were TUNEL positive in KD-Scr. Nuclease treatment was used to create nicked DNA as a positive control.

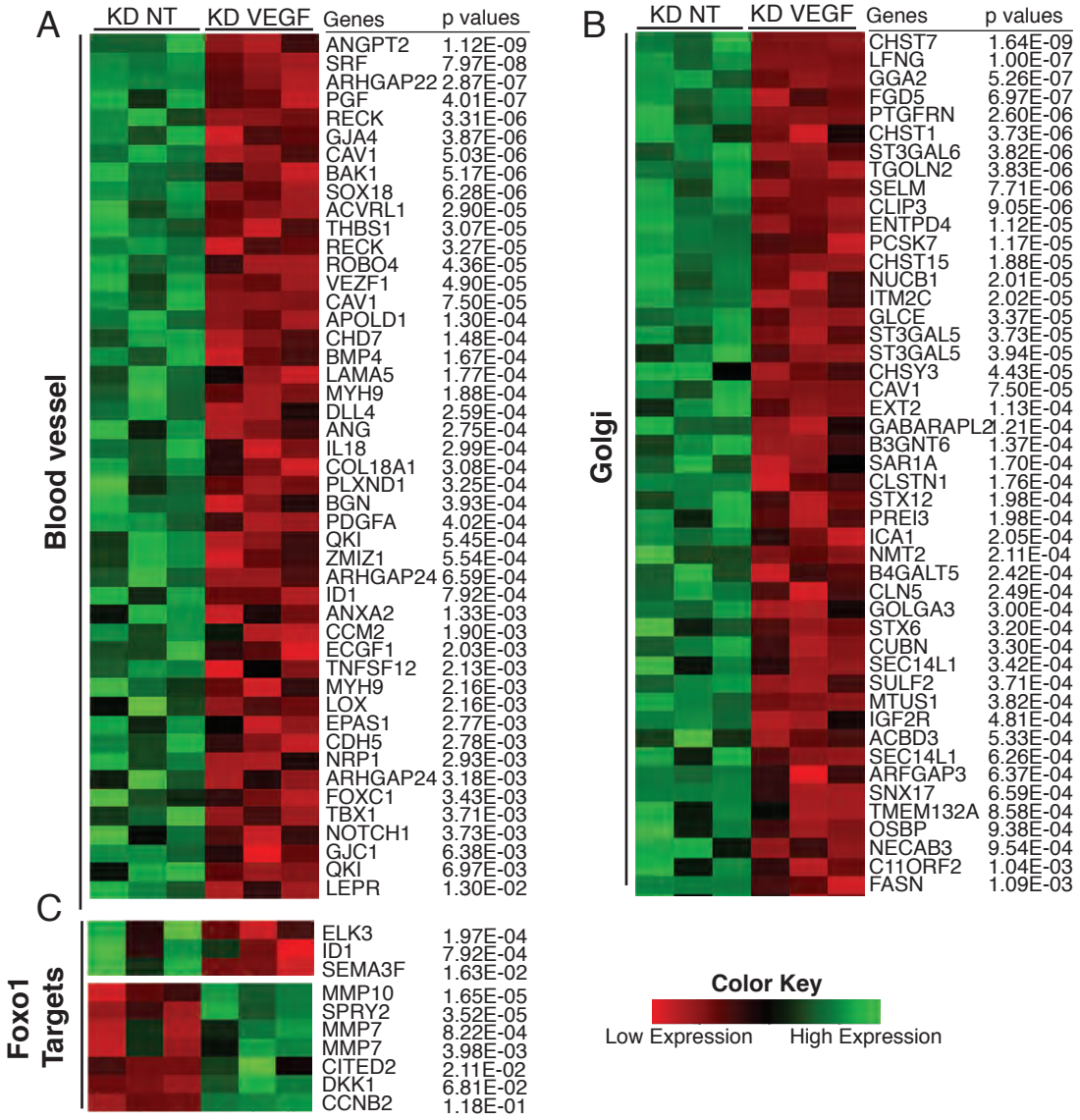

Supplemental Figure 2: Autocrine VEGF is required to maintain endothelial identity, mitochondrial and Golgi transcriptome

HUVECs were transfected with siRNA targeting VEGF and total RNA was isolated on day 4 after first transfection (n=3). Gene expression profile was assessed with Illumina human gene chip expression assay. GO clusters extracted from genes significantly up- and down-regulated in KD-VEGF analyzed by DAVID. Heatmaps highlight a subset of two down-regulated GO clusters: (A) blood vessel and (B) Golgi. (C) Select Foxo1 targets significantly up- or down-regulated.

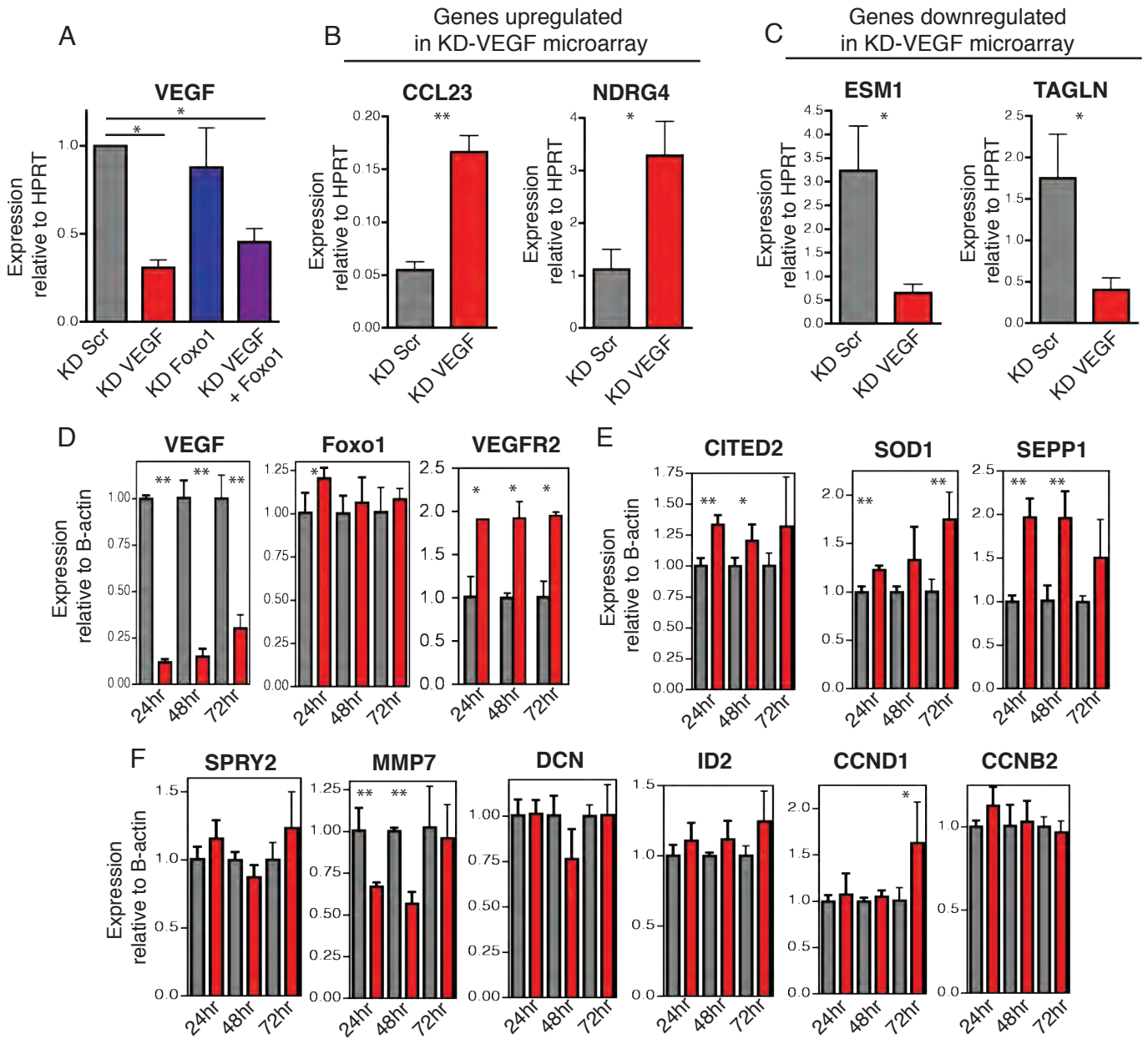

Supplemental Figure 3: Microarray validation and further analysis of Foxo1 target genes

(A) A significant decrease in VEGF levels was maintained in double-knockdown conditions. Two of the top genes found (B) increased (CCL23 and NDRG4) and (C) decreased (ESM1 and TAGLN) in the KD-VEGF condition of the microarray were validated by RT-PCR. (D) RT-PCR analysis of several genes of interest showed that decrease in VEGF levels was maintained over several days, Foxo1 levels remained largely unchanged, and VEGFR-2 levels were drastically increased. Several previously-described Foxo1 targets were found to be (E) increased as expected in the KD-VEGF condition by RT-PCR (CITED2, SOD2, SEPP1) or (F) found to be unchanged or regulated contrary to previous reports (SPRY2, MMP7, DCN, ID2, CCND1, CCNB2).

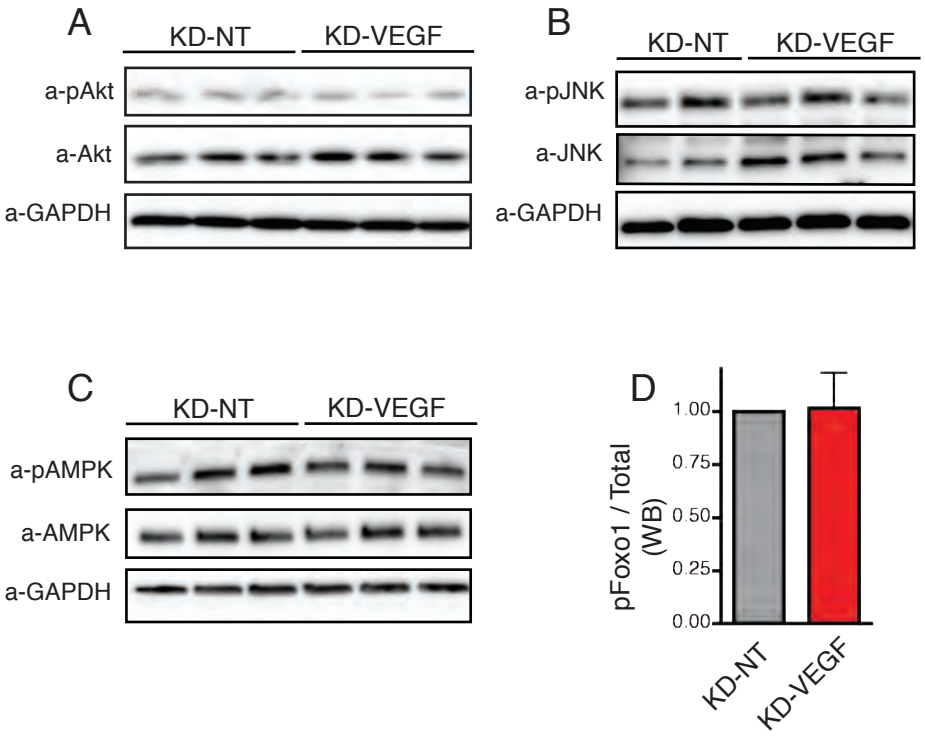

Supplemental Figure 4. No changes observed in signaling pathways upstream of Foxo1 or in phospho-Foxo1 levels. Western blots investigating the phospo- activation status of (A) Akt, (B) JNK and (C) AMPK were performed, revealing no significant differences between KD-VEGF and KD-NT conditions. (D) Western blots were performed and quantified showing phospho-Foxo1 status was unchanged relative to total Foxo1 protein in KD-NT and KD-VEGF HUVECs.

Table S1 – DAVID analysis of genes significantly downregulated in KD-VEGF

GO Cluster	Term	Count	Benjamini	Fold Enrichment
Cluster 1 – Enrichment Score: 9.02				
	Golgi apparatus	128	8.53E-09	1.78
	GO:0005794-Golgi apparatus	175	4.96E-07	1.54
	GO:0044431-Golgi apparatus part	75	1.88E-06	1.96
Cluster 2 – Enrichment Score: 6.88				
	GO:0001568-blood vessel development	65	3.66E-05	2.08
	GO:0001944-vasculature development	65	5.01E-05	2.03
	GO:0048514-blood vessel morphogenesis	54	8.71E-04	2.01
	GO:001525-angiogenesis	41	2.17E-03	2.17
Cluster 3 – Enrichment Score: 6.21				
	endoplasmic reticulum	146	2.91E-08	1.67
	GO:0005783-endoplasmic reticulum	179	2.75E-05	1.43
	GO:0044432-endoplasmic reticulum part	64	6.67E-02	1.42
Cluster 4 – Enrichment Score: 5.12				
	IPR001849:Pleckstrin homology	65	2.11E-03	1.86
	domain:PH	56	2.59E-03	1.92
	SM00233:PH	65	1.79E-03	1.76
	IPR011993:Pleckstrin homology-type	60	2.22E-01	1.57
Cluster 5 – Enrichment Score: 4.07				
	nucleotide binding	278	5.93E-06	1.35
	atp-binding	226	8.02E-06	1.39
	transferase	232	3.14E-05	1.36
	kinase	129	3.80E-05	1.53
	GO:0000166-nucleotide binding	356	4.81E-03	1.24
	GO:0001882-nucleoside binding	261	1.56E.02	1.26
	GO:0001883-purine nucleoside binding	259	1.18E-02	1.26
	GO:0030554-adenyl nucleotide binding	255	1.05E-02	1.26
	GO:0005524-ATP binding	240	1.12E-02	1.27
	GO:0032559-adenyl ribonucleotide binding	242	1.24E-02	1.26
	GO:0006793-phosphorus metabolic process	165	2.43E-02	1.33
	GO:0006796-phosphate metabolic process	165	2.43E-02	1.33
	GO:0004672-protein kinase activity	111	1.60E-02	1.43
	binding site: ATP	98	6.76E-02	1.47
	GO:0017076-purine nucleotide binding	299	1.42E-02	1.21
	GO:0032555-purine ribonucleotide binding	286	1.72E-02	1.21
	IPR017441:Protein kinase, ATP binding site	85	1.72E-02	1.48
	active site: proton acceptor	113	2.07E-01	1.40
	domain: Protein kinase	84	1.35E-01	1.46
	IPR000719:Protein kinase, core	86	1.90E-01	1.43
	IPR002290:Serine/threonine protein kinase	52	2.30E-01	1.59
	Nucleotide phosphate-binding region:ATP	152	2.63E-01	1.28
	serine/threonine-protein kinase	69	3.41E-01	1.48
	GO:0016310-phosphorylation	132	2.82E-02	1.29
	GO:0006468-protein amino acid phosphorylation	112	1.30E-01	1.32
	GO:0004674-protein serine/threonine kinase	77	1.58E-01	1.39
	SM00220:S_TKc	52	1.15E-01	1.51
	IPR008271: Serine/threonine protein kinase	64	2.05E-01	1.43
	IPR017442: Serine/threonine protein kinase-rela	64	4.99E-01	1.41

Table S2 – DAVID analysis of genes significantly upregulated in KD-VEGF

GO Cluster	Term	Count	Benjamini	Fold Enrichment
Cluster 1 – Enrichment Score: 18.55				
	Mitochondrion	200	3.39E-21	2.03
	GO:0005739-mitochondrion	243	1.36E-20	1.85
	transit peptide	125	4.79E-16	2.22
	transit peptide: Mitochondrion	123	2.66E-14	2.22
	GO:0044429-mitochondrial part	134	3.25E-11	1.86
Cluster 2 – Enrichment Score: 13.68				
	GO:0031974-membrane enclosed lumen	352	2.15E-18	1.57
	GO:0070013-intracellular organelle lumen	339	4.91E-18	1.57
	GO:0043233-organelle lumen	342	2.61E-17	1.55
	GO:0031981-nuclear lumen	272	7.67E-13	1.55
	GO:0005654-nucleoplasm	175	6.55E-10	1.64
	GO:0005730-nucleolus	131	6.49E-06	1.55
	GO:0044451-nucleoplasm part	106	3.60E-05	1.58
Cluster 3 – Enrichment Score: 8.86				
	GO:0030529-ribonucleoprotein complex	142	1.20E-19	2.28
	ribonucleoprotein	90	4.56E-17	2.73
	ribosomal protein	65	9.91E-14	2.92
	GO:0006412 – translation	95	3.14E-11	2.27
	GO:0005840 – ribosome	69	1.55E-12	2.65
	GO:0033279-ribosomal subunit	48	3.28E-11	3.10
	GO:0003735-structural constituent of ribosome	57	4.70E-10	2.76
	protein biosynthesis	48	1.87E-05	2.16
	GO:0015934-large ribosomal subunit	25	1.30E-05	3.08
	hsa03010: ribosome	30	3.46E-04	2.53
	GO:0006414-translational elongation	31	6.85E-04	2.43
	GO:0022626-cystolic ribosome	25	4.13E-04	2.55
	GO:0044445–cystolic part	37	9.77E-04	2.01
	Ribosome	22	1.81E-03	2.55
	GO:0022625-cystolic large ribosomal subunit	14	5.09E-03	3.04
	GO:0022627-cystolic small ribosomal subunit	11	1.71E-01	2.27
	GO:005198-structural molecule activity	89	8.50E-01	1.14
Cluster 4 – Enrichment Score: 8.85				
	GO:0000278-mitotic cell cycle	97	2.15E-09	2.07
	GO:0007049-cell cycle	167	4.24E-08	1.65
	Mitosis	54	1.87E-08	2.50
	GO:0022403-cell cycle phase	98	3.96E-07	1.87
	cell cycle	101	5.33E-08	1.85
	GO:0022402-cell cycle process	123	4.49E-07	1.72
	GO:0048285-organelle fission	64	4.05E-07	2.21
	GO:0000087-M phase of mitotic cell cycle	62	1.03E-06	2.19
	Cell division	66	2.72E-07	2.11
	GO:0000279-M phase	80	2.70E-06	1.92
	GO:0007067-mitosis	60	2.91E-06	2.16
	GO:0000280-nuclear division	60	2.91E-06	2.16
	GO:0051301-cell division	68	2.25E-04	1.82

Table S3 – DAVID analysis of genes following Expression Pattern 1

GO Cluster	Term	Count	Benjamini	Fold Enrichment
Cluster 1 – Enrichment Score: 3.67				
	GO:0022402-cell cycle process	43	6.85E-03	2.17
	GO:0022403-cell cycle phase	34	9.64E-03	2.34
	GO:0000278-mitotic cell cycle	31	1.19E-02	2.39
	GO:0007049-cell cycle	50	2.16E-02	1.84
	GO:0000279-M phase	27	3.91E-02	2.34
	GO:0000087-M phase of mitotic cell cycle	20	9.66E-02	2.55
	GO:0048285-organelle fission	20	1.12E-01	2.49
	GO:0000280 nuclear division	19	1.59E-01	2.46
	GO:0007067-mitosis	19	1.59E-01	2.46
	Cell cycle	30	4.49E-02	1.97
	GO:0051301-cell division	22	2.74E-01	2.13
	cell division	19	1.16E-01	2.18
	mitosis	15	1.07E-01	2.48
Cluster 2 – Enrichment Score: 3.10				
	ribonucleoprotein	27	4.60E-04	2.93
	ribosomal protein	19	5.86E-03	3.06
	GO:0005840-ribosome	20	1.58E-02	2.75
	GO:0030529-ribonucleoprotein complex	34	2.37E-02	1.95
	GO:0033279-ribosomal subunit	14	2.37E-02	3.23
	GO:0003735-structural constituent of ribosome	16	4.19E-01	2.75
	GO:0006412-translation	23	3.17E-01	1.98
	hsa03010:Ribosome	8	9.95E-01	2.24
	GO:0005198-structural molecule activity	23	9.94E-01	1.05
Cluster 3 – Enrichment Score: 2.61				
	GO:0005739-mitochondrion	65	2.75E-03	1.77
	GO:0044429-mitochondrial part	42	2.08E-03	2.08
	Mitochondrion	48	1.79E-02	1.74
	Transit peptide: mitochondrion	30	7.81E-01	1.93
	GO:0031090-organelle membrane	57	5.12E-02	1.54
	Transit peptide	30	5.81E-02	1.91
	GO:0031966-mitochondrial membrane	25	1.07E-01	1.87
	GO:0005740-mitochondrial envelope	26	1.01E-01	1.83
	GO:0031980-mitochondrial lumen	17	9.89E-02	2.21
	GO:0005759-mitochondrial matrix	17	9.89E-02	2.21
	GO:0031967-organelle envelope	33	1.68E-01	1.57
	GO:0031975-envelope	33	1.67E-01	1.57
	GO:0005743-mitochondrial inner membrane	17	4.22E-01	1.64
	GO:0019866-organelle inner membrane	17	5.50E-01	1.53
	Mitochondrion inner membrane	11	6.46E-01	1.72
Cluster 4 – Enrichment Score: 2.34				
	GO:0051726-regulation of cell cycle	26	8.71E-02	2.24
	GO:0010564-regulation of cell cycle process	12	2.96E-01	3.00
	GO:0007346-regulation of mitotic cell cycle	14	3.29E-01	2.63
	GO:0007093-mitotic cell cycle checkpoint	7	3.48E-01	4.65
	GO:0000075-cell cycle checkpoint	9	5.34E-01	2.82
	GO:0031575-G1/S transition checkpoint	3	9.15E-01	5.04
Cluster 5 – Enrichment Score: 2.32				
	GO:0005761-mitochondrial ribosome	8	5.48E-02	4.92
	GO:0000313-organellar ribosome	8	5.48E-02	4.92
	GO:0005763-mitochodrial small ribosomal	4	2.35E-01	6.56

GO:0000314-organellar small ribosomal	4	2.35E-01	6.56

Table S4 – DAVID analysis of genes following Expression Pattern 2

GO Cluster	Term	Count	Benjamini	Fold Enrichment
Cluster 1 – Enrichment Score: 5.70				
	GO:0048514-blood vessel morphogenesis	23	1.00E-03	3.60
	GO:0001568-blood vessel development	24	1.75E-03	3.23
	GO:0001944-vasculature development	24	1.77E-03	3.15
	GO:0001525-angiogenesis	17	5.94E-03	3.79
Cluster 2 – Enrichment Score: 4.33				
	GO:0016477-cell migration	24	5.16E-03	2.87
	GO:0048870-cell motility	24	2.30E-02	2.58
	GO:0051674-localization of cell	24	2.30E-02	2.58
	GO:0006928-cell motion	31	3.71E-02	2.15
Cluster 3 – Enrichment Score: 2.23				
	hsa04360:Axon guidance	14	1.13E-01	2.94
	domain: Sema	6	5.97E-01	6.50
	IPR002165: Plexin	6	6.38E-01	6.36
	IPR001627:Semaphorin/CD100 antigen	6	6.38E-01	6.36
	IPR003659: Plexin/semaphorin/integrin	7	4.97E-01	5.11
	SM00630:Sema	6	5.93E-01	5.60
	SM00423:PSI	7	3.89E-01	4.50
	IPR015943:WD40/YVTN repeat-like	15	9.47E-01	1.64
	Domain:Ig-like C2-type	5	1.00E+00	1.63
Cluster 4 – Enrichment Score: 1.83				
	IPR013761:Sterile alpha motif-type	10	3.81E-01	4.27
	IPR001660:Sterile alpha motif-SAM	9	8.11E-01	3.18
	SM00454:SAM	9	6.85E-01	2.80
	domain:SAM	7	9.59E-01	2.90
	IPR011510:Sterile alpha motif homology 2	3	9.98E-01	2.40
Cluster 5 – Enrichment Score: 1.74				
	GO:0030054-cell junction	26	7.19E-01	1.67
	cell junction	21	3.46E-01	1.78
	GO:0005911-cell-cell junction	12	6.30E-01	2.10
Cluster 6 – Enrichment Score: 1.73				
	actin-binding	16	2.07E-01	2.19
	GO:0008092-cytoskeletal protein binding	26	7.74E-01	1.67
	GO:0015629-actin cytoskeleton	16	6.39E-01	1.97
	GO:0003779-actin binding	16	9.44E-01	1.59
Cluster 7 – Enrichment Score: 1.63				
	GO:0001667-ameboidal cell migration	6	6.73E-01	5.35
	GO:0014032-neural crest cell development	5	7.91E-01	5.00
	GO:0014033-neural crest cell differentiation	5	7.91E-01	5.00
	GO:0060485-mesenchyme development	6	8.10E-01	3.81
	GO:0001755 neural crest cell migration	4	8.08E-01	5.74
	GO:0014031-mesenchymal cell development	5	8.54E-01	3.23
	GO:0048762-mesenchymal cell differentiation	5	8.54E-01	3.23